

MODELLING OF THE STATIC AND DYNAMIC PROPERTIES OF THO-TYPE SILICATES

REUBEN CAUCHI AND JOSEPH N. GRIMA

*Department of Chemistry, Metamaterials Unit
Faculty of Science, University of Malta
Msida MSD 2080, Malta*

(Received 3 January 2014; revised manuscript received 15 February 2014)

Abstract: Auxetic materials are materials exhibiting a negative Poisson's ratio in one of their planes. This phenomenon has been studied in various materials. Zeolites are crystalline substances whose structure is characterised by the framework of linked tetrahedra, each consisting of four oxygen atoms surrounding a cation. The resulting interstitial spaces make them efficient for use as adsorbents and molecular sieves, and many studies have been focused on this aspect. Some of these zeolites may exhibit auxeticity at least in one of their planes. THO (and similar systems, such as NAT and EDI) together with the all-silica equivalent of these have been studied extensively via static simulations for their negative Poisson's ratio in the (001) plane.

In this paper a study of the all-silica equivalent of THO has been carried out via both static and dynamic simulations using the same force-field, where the system was subjected to stress along the x direction. The hypothesised semi-rigid mechanism of deformation, proposed by Grima *et al.* was then projected over this framework. The results obtained confirmed auxeticity along this plane by means of the COMPASS force-field, in both static and dynamic studies and compared well with the proposed mechanism of semi-rigid rotating polygons. It also showed that as the Young's modulus of this mechanism increases other mechanisms of deformation increase in importance.

Keywords: auxetics, zeolites, thomsonite, molecular dynamics

1. Introduction

One normally expects that when a material is uniaxially stretched, a lateral compression is observed, while when it is uniaxially compressed a lateral expansion is observed. Nevertheless, not all materials behave like this. In fact, opposing this commonly observed phenomenon are auxetic materials which show a lateral expansion upon uniaxial stress and a lateral compression upon strain [1]¹.

1. Apart from auxetic behaviour, other interesting features may be observed in certain materials, including: negative stiffness [2], negative compressibility [3] and negative thermal

The extent of change in lateral dimension when a material is uniaxially stretched or compressed is measured through the Poisson's ratio. In particular, for a material being loaded in the Ox_i , then the Poisson's ratio ν_{ij} in the $Ox_i - Ox_j$ plane (where Ox_j is perpendicular to Ox_i) is defined as:

$$\nu_{ij} = \frac{-\varepsilon_j}{\varepsilon_i} \quad (1)$$

where ε_i and ε_j are the applied and resulting strain in the Ox_i and Ox_j directions respectively. For a conventional material, a positive strain ε_i (stretching in Ox_i) is accompanied by a negative strain ε_j (material gets thinner) resulting in an overall positive Poisson ratio. However in auxetic materials, a positive strain ε_i (stretching in Ox_i) is accompanied by a positive strain ε_j (material gets fatter) resulting in an overall negative Poisson ratio (NPR) [1]. Another interesting group of materials are those with an overall zero Poisson ratio, like cork, which show no lateral expansion or contraction when the material is stretched or compressed [6].

It is now known that auxeticity is a phenomenon which may be observed in a variety of materials. The way it arises in a particular material is dependent on the way that particular features in the material's micro or nanostructure deforms when subjected to a load (the deformation mechanism). In other words, the geometry of the micro/nano structure plays an important role in defining the Poisson ratio [7]. In this respect it should be noted that the geometry/deformation mechanisms that lead to particular values of the Poisson's ratios are independent from the scale of structure and in the past decade, it became common practice to use macroscaled models to ease examination and explanation² of the interplaying mechanisms that lead to the deformation of the geometry at the micro and nano scale.

It should be noted that the mechanism by which the phenomenon of negative Poisson ratio comes about is more eluding than the geometrical unit responsible for it since the geometry can usually be easily experimentally determined through microscopy whilst the experiments required to view deformation mechanism acting at the nano/micro scale are more complex to perform. For example, it was only very recent that experimental work using CT scans was performed to verify the deformation mechanisms which result in negative Poisson's ratios in auxetic foams [8] whilst so far no actual experimental work was done at the nanoscale. Such added complexity may be better appreciated when one realises that, upon stress, systems having the same geometrical features may respond through a different mechanism, possibly resulting in different Poisson ratios to the extent that sometimes there is even a difference in sign of the Poisson ratio. This is clearly manifested in re-entrant honeycombs [9–11] which are known to be

expansion [4]. The latter is an interesting feature observed in a number of materials and structures, including zeolites [5].

2. Micro and nano scale structures are usually found in materials, such as foams and metals or crystals, respectively.

auxetic if they deform through flexure of the ribs or hinging of the cell walls but conventional if they deform through stretching of the cell walls (see Figure 1). Further complications in explaining auxeticity in molecular/microscale systems may arise since their geometry tend to deviate from that of the equivalent idealised macroscale model. This can in fact be observed in zeolites where the rigid rotating polygons model is not perfectly valid to describe their behaviour at the molecular level. Instead a semi-rigid geometry is observed [12].

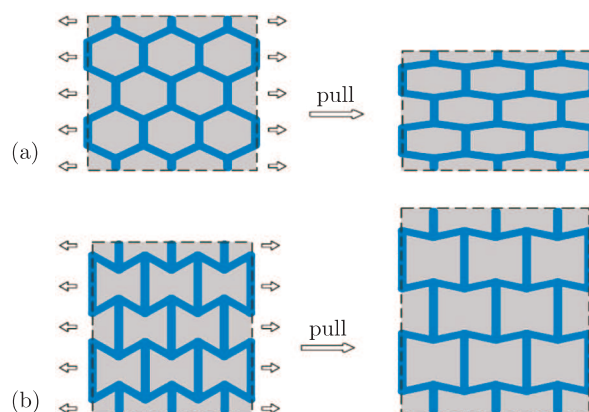


Figure 1. (a) Shows the conventional honeycomb structure – positive Poisson’s ratio; (b) shows the re-entrant structure – negative Poisson’s ratio; and deformation upon stress (picture taken from [13])

This paper will focus on studies of the Poisson’s ratios in idealised fully siliceous zeolite frameworks in particular, the SiO_2 equivalent of the thomsonite (THO) framework. Zeolites are crystals made up of oxygen, aluminium and silicon, together with cations, such as sodium and calcium, present within the porous structure. Siliceous zeolites are zeolites which have silicon instead of aluminium in there structure, cations may be absent from the pores within the structure. Through the Poisson’s ratios such materials have been studied quite extensively by computer simulations [14, 15, 12, 16–19] and even experimental work [20], the deformation mechanisms have so far always been studied through force-based static modelling which is inferior to dynamics. Dynamic analysis gives a more detailed picture of the actual mechanisms occurring in the structure under a set of defined conditions as they also include the parameters of time and temperature which cannot be included in static calculations.

More specifically, this paper will thus examine literature available on such structures (Section 2). This is followed through a static study of siliceous THO using the COMPASS force-field (Section 3) followed by a dynamic analysis (Section 4). These simulations were aimed at obtaining further evidence on the auxeticity and deformation mechanism in the siliceous THO and, more importantly, in order to provide ground for further dynamic analysis on similar structures which have not yet been analysed by dynamic simulations.

2. Literature review

This section has three main subsections, the first of which discusses the relevant literature relating to auxetic materials. In particular, structural models which exhibit auxeticity at the macrolevel are presented together with auxetic micro-structured materials and molecular systems as well as possible applications for such systems. In the second part of this review, the different modelling techniques that are used in this work are discussed followed by a final section which includes a brief review on zeolites and siliceous zeolites

2.1. Auxetic materials and structures

Auxeticity may occur at the macro, micro or nano level. The specific spatial arrangement of geometrical features and their resultant net displacement, resulting from the interplay of different deformation mechanisms, may result in the material exhibiting a negative Poisson's ratio. Thus this treatise on auxetic materials will deal with the geometrical arrangements of these units, illustrated with examples at the relevant scale and a general overview of some of the mechanisms which interplay within the structures.

2.1.1. Mechanism and structures of auxeticity

In this section a literature review of the mechanisms of auxeticity observed or hypothesised within a number of real or hypothesised structures will be discussed.

2.1.1.1. Hinging/flexing

Models deforming through hinging and flexing were among the first to be proposed for their auxetic behaviour. In these mechanisms part of the unit hinges or flexes such that the structure expands both along the direction of loading and in a perpendicular direction. Hinging mechanism in general involves the relative rotation of two linked entities within the basic unit while flexing involves the bending of the beam-like entity. Various geometrical structures, listed below may be auxetic by such mechanisms.

Re-entrant (Honeycomb)

Possibly one of the first geometrical structures to be described, it consists of hexagonal honeycombs with the two vertices opposing each other pointing towards the centre of the honeycomb.

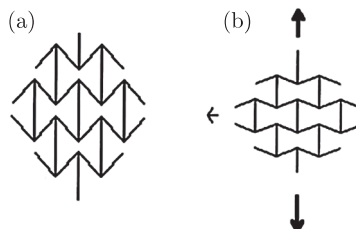


Figure 2. (a) The re-entrant honeycomb structure; (b) auxetic nature upon application of stress [21]

This leads to a structure which may exhibit a negative Poisson ratio, depending on the mechanism which takes place upon application of stress. Hinging, flexing, dilating, or a combination of these mechanisms may interplay in deformation of both conventional and re-entrant honeycombs, resulting in auxetic or non-auxetic behaviour [9–11]. When re-entrant honeycombs deform through dilation alone they exhibit a positive Poisson ratio, while hinging and/or flexing results in a negative Poisson ratio. On the other hand conventional honeycombs exhibit opposite directions of Poisson ratio with the respective mechanisms. The degree of auxeticity depends also on the length and width of the ribs and the initial value of the angle between them [22].

A notable example where conventional honeycombs were found to exhibit auxetic behaviour was in graphene sheets by Scarpa and co-workers, which considered the system as not just rigid trusses with hinges, but rather as trusses being able to undergo deformations by stretching, thus as one may note from the figure below, upon shearing of the hexagonal structure, the bond results in not only hinging but stretching as well, thus resulting in an increase in volume of the hexagon along both perpendicular directions.

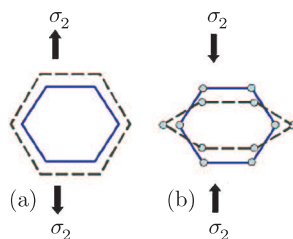


Figure 3. Conventional honeycomb deforming upon stress by flexing and hinging resulting in a negative Poisson ratio (image from [23])

Polyphenylacetylene system

The polyphenylacetylene system, is probably a classical example of a nano-scale re-entrant honeycombs; Acetylene chains connect units of 1,2,3-trisubstituted benzene rings together, forming the structure below;

A similar polyacetylene based structure was proposed by Baughman, instead of having phenyl rings acting as hinges, the hinges are made of sp^2 – sp^2 single bonds in polyacetylene chains, which allow for hinging of the bonds. These chains form networks termed as twisted chain auxetics, or (10,3)-*b* networks, allow for shear deformation along the helical polyacetylene chains, resulting in an auxetic behaviour. [25, 26]

Foams

These are interesting materials, with a wide array of implementation in industry. Conventional foams, having a positive Poisson' ratio may be converted to auxetic foams by two methods. The first method developed involved heating beyond the foam polymers' softening temperature, and placing a volumetric compression on the foam, and then allowed to cool while still compressed [27, 28].

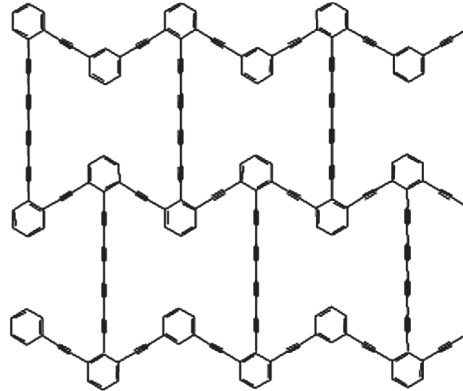


Figure 4. The polyphenylacetylene structure showing a re-entrant honeycomb (image adopted from [24])

A later method developed by Grima and co-workers involve compression of the conventional foam and immersing in acetone for about an hour, then allowing to dry, while still compressed. Foams formed by this method are known to revert back into a conventional material, with no auxeticity [29].

The mechanism by which these auxetic foams deform is an eluding one, with a number of proposed mechanisms. Modelling of the microstructure of foams is a major issue, usually modelled on hexagonal honeycombs [30, 10], it has been proposed that the auxetic equivalents have the Y shaped joint inverted into re-entrant arrows, similar to the concept proposed by Lakes resulting in a re-entrant honeycomb (Figure 5).

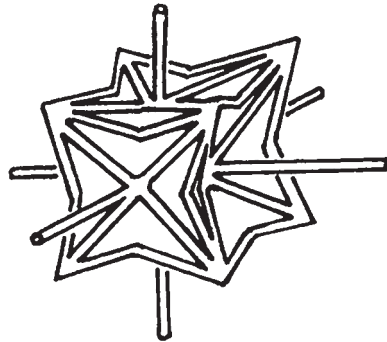


Figure 5. The idealised cell structure proposed by Lakes (1987) formed from a 24-sided collapsed polyhedron with a cubic symmetry

Bowtie Structure

This mechanism is usually observed in prismanes and arises within the inner rings of the structure, while the outer rings are conventional and not auxetic the inner rings exhibit auxeticity. [31] It was found that the auxeticity arises from the bond arrangements of the sp^3 hybridised bonds forming the carbon rings

within the prismanes. The angles in the tetrahedral arranged carbons forming the prismane are arranged according to the number of carbons within the ring. According to the Thorpe-Ingold effect, the contraction of one angle results in opening of another angle [32], as noted in the figure below, two bonds from one carbon form the ring, while another two bonds join up the rings together forming a sort of midrib. The larger the ring the larger is the angle forming these ribs, and thus the more pronounced is an effect in the change of these angles, resulting in a geometrical structure which is more similar to a bowtie, and hence a more pronounced negative Poisson ratio is observed on an increase in the ring size. Also a change in atoms, either forming the ring, or bonded to carbon will result in a different affect, showing the affect of substituents on mechanical properties [32].

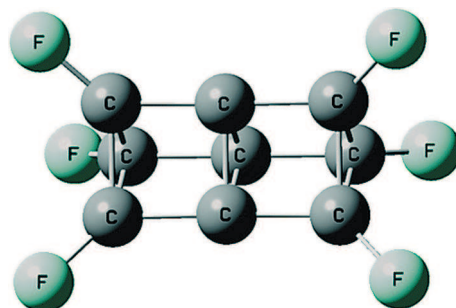


Figure 6. Figure of a prismane structure whose inner ring is made up of 3 carbon atoms, with substituents on the end carbon rings [32]

Star-n system

This star- n system is a system whereby the presence of a star-shaped unit is the basis for this unusual behaviour; various authors, such as Attenborough 1997, have proposed structures equivalent or similar to this [33]. The generic name for such a system was coined by Grima and co-workers where it was noted that arms of an arrow-shaped basic unit, connect together, forming stars, see figure below. The points of the stars, or the ribs connected to each point, denote the value of n in the name of the system. When $n = 3, 4, 6$, it was noted that auxetic behaviour is observed [33].

Microporous Polymers

These molecules are exemplified mainly by PTFE (polytetrafluoroethylene), their structure is composed of nodules and fibrils, resulting in an interconnecting network, similar to some extent to a honeycomb structure. One of the interesting features of these materials is their highly negative Poisson's ratio, as large as -12 [34]. The material is highly anisotropic, and the auxeticity is thought to arise via two possible mechanisms, both involving the principle that the fibrils, upon stress, tense, and push the nodules apart. One mechanism may be explained as similar to rotating rectangle, the nodules, pulled by strings, the fibrils [34], this system has the highest Poisson ratio, of -12 . The other mechanism involves node

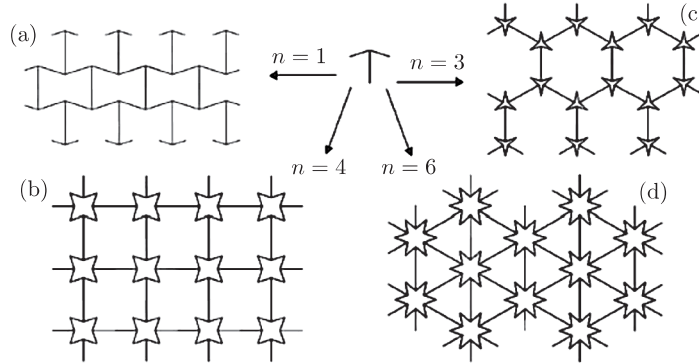


Figure 7. Some tessellations constructed from an arrow sub unit. When $n = 1, 3, 4, 6$ (a), STAR-3 system (b), STAR-4 system (c) and STAR-6 system (d) are formed, respectively (image adopted from [33])

translation, where the node moves and the hinging angles change, such a system was found to have a Poisson ratio of -6 [35]. A number of other materials inspired by such a polymer have been produced and tested; examples include ultra high weight poly-ethylene [UHMWPE] [36, 37] and others.

2.1.1.2. Egg rack mechanism

First proposed as a macrostructure, it literally based on an egg container and exhibits auxetic behaviour when loaded in a way similar to that of cubic metals. The principle is that of an umbrella with four spokes, each bound to three other spokes, forming another umbrella-like unit, the points though; alternate; one pointing down and the other upwards resulting in the structure shown in the Figure 8.

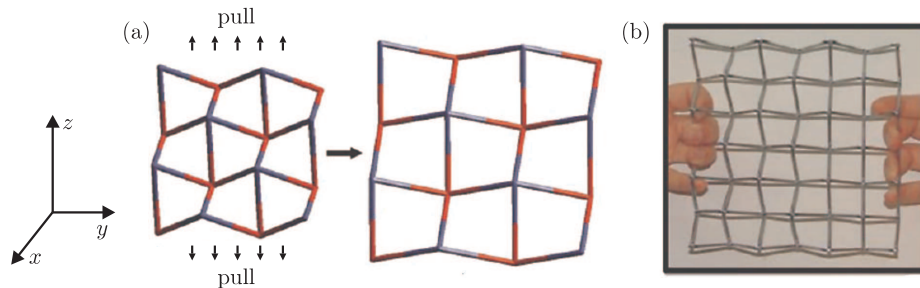


Figure 8. Image depicting the macrostructure of the egg rack mechanism and its deformation after stress (image from [38])

Pulling along any direction results in the opening of these umbrella-like units leading to a negative and isotropic Poisson's ratio of -1 . In fact, mechanical tests on a real metal egg rack structure gave Poisson's ratios $v_{23} = v_{32} = -1.02 \pm 0.04$ [38].

This model is not scale-specific and it was downscaled to the molecular level with calixarenes as the basic unit. As seen in the figure below, these consist

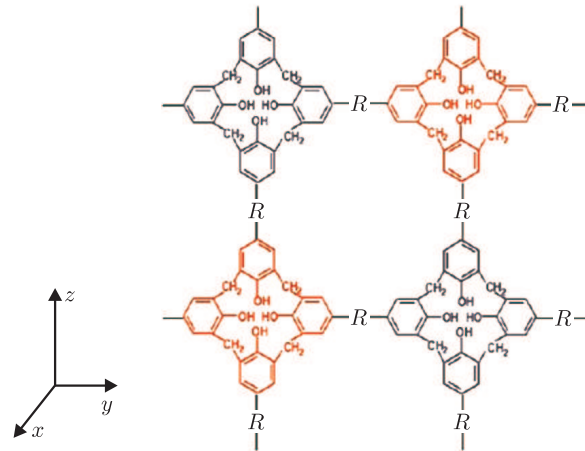


Figure 9. Figure showing the molecular structure of a calix-[4]-arene (the 4 indicates the number of aromatic rings in the cup-like structure, this is variable and replaced by n for a generic calyx[n]arene; R could be: (a) none, (b) phenyl) (image from [38])

of aromatic rings with a hydroxyl group facing other hydroxyl groups. This configuration results in a nanoscopic configuration similar to a cup.

The structure exhibits a similar geometric structure, were the apex of the cup is the aforementioned point of the umbrella, and each unit of calixarene may be arranged in an alternating method;

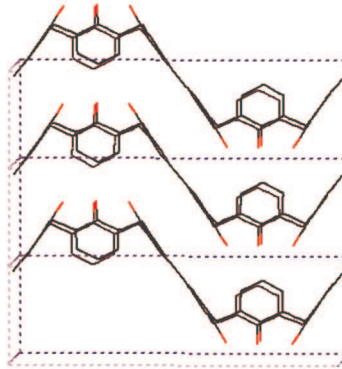


Figure 10. Image showing the alternating structure of the apex in the calix-4-arene (image from [39])

A more recent example of another molecular system is that of a highly oriented carbon nanotube structure, proposed by Luzhuo Chen, as one may note from the diagram below the structures are similar to an egg-rack model, and they are estimated to have a Poisson ratio of about -0.5 .

Cubic Metals

Auxeticity in these metals is observed along a specified direction, as observed from figure 2.4 below; when a tensile strength is applied along the [110]

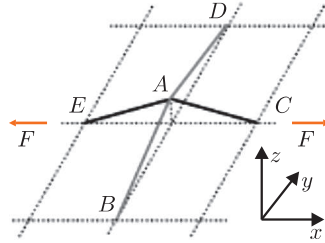


Figure 11. The hypothetical arrangement of the carbon nanotubes, resembling an egg-rack structure [40]

direction, the acute angles of the rhombus, defined by atoms 1, 2, 3 and 1, 4, 3 decrease in size, resulting in an increase in the angle size of the bonds bonded to atoms 3 and 1, this results in the acute bond angles of atoms, 1, 3 and 1, 5, 3, decreasing in size, causing an elongation in the crystal along the [110] and [10] directions, without increasing the nearest-neighbour separation. Thus pushing of atoms 5 and 6 apart due to separation of atoms 1 and 3 results in a negative ν (110,10).

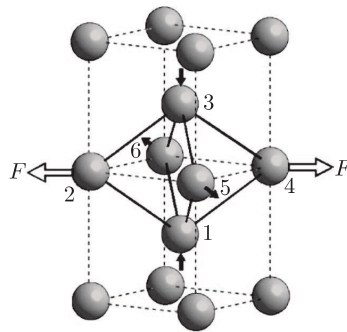


Figure 12. A cubic metal showing the auxetic mechanism taking place upon stress in the specified direction (image from [3])

2.1.1.3. Chiral units

In this system the most important feature are not just the point connections, but also the ribs by which the units are connected. The ribs must be flexible such that the changes occurring due to external forces result in predominantly flexing the interconnecting ribs.

The term chiral system arose from the first proposed geometrical structures exhibiting a negative Poisson ratio via flexure of their interconnecting rods, [41], The model implemented by Lakes in 1991 involved a 2D periodic hexagonal chiral structure [42]. The basic unit was a central cylinder (node) with six tangential ligaments, linking to other units in the structure. The nodes may not necessarily be cylindrical since the ability for the links to flex is responsible for the Poisson ratio observed; geometrical shapes for nodes described include also squares and triangles.

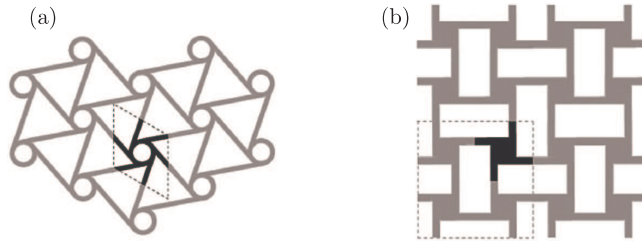


Figure 13. (a) Chiral honeycombs proposed by Lakes (1991) and (b) the ‘anti-tetrachiral’ network proposed by Sigmund and coworkers (1998) note the basic units are in black (image from [43])

The namesake for this system is the chirality of the interconnections between nodes, if all nodes have ribs connecting along the same direction then the system is termed chiral, while if the nodes are connected by ribs which mirror each other, than the system is termed antichiral (Figure 14).

It was later observed that the models proposed by Lakes and Sigmund were actually examples of a number of possible structures one may construct from the building blocks which make these structures. It was shown that an infinite amount of these units may be produced upon combination of various factors, including the chirality and the order of symmetry of these blocks [43].

Assuming only a periodic structure of rotational symmetry n in its building blocks, only systems were $n = 3, 4,$ or 6 may be used, as seen from the diagram below.

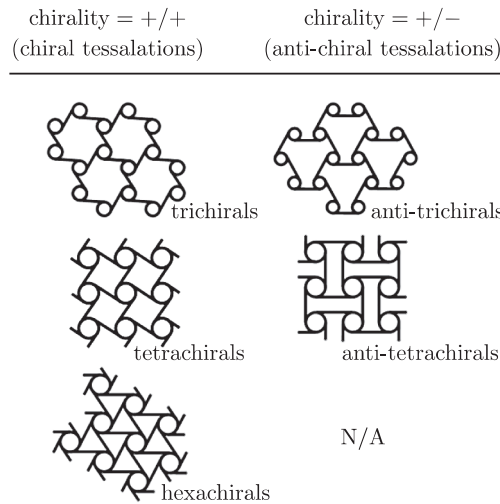


Figure 14. The five tessellations obtainable for chital subunits with a symmetry of order n if the symmetry restraints are relaxed more units may be obtained (image from [43])

This work also introduced the concept, of meta-chirals, where, as one may observe from the figure below, the network has two different types of connection

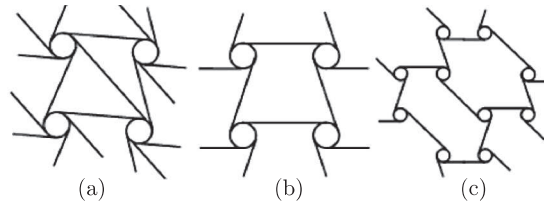


Figure 15. If symmetry restraints are relaxed more chiral sub units may be obtained, with structures not necessarily having chirality and not necessarily having a symmetry of order n [43]

i.e. both chiral and antichiral while symmetry restraints on nodes are relatively relaxed.

As one may note from the above diagrams, when one pulls longitudinally on the structure, the ribs flex and pull the nodes, the transverse ribs thus also are caused to flex bringing on an expansion in both directions.

2.1.1.4. Rotating auxetics

As the name itself indicates, the mechanism within such structures involves a rotating unit. Sigmund was the first to propose such a system, his tessellatable unit involved the two superimposed quadratic frames, which are able to rotate around the centre. When an expansion occurs in one direction, the units rotate around the centre at an opposite direction resulting in an expansion in the later direction as well, and thus in a negative Poisson ratio [44].

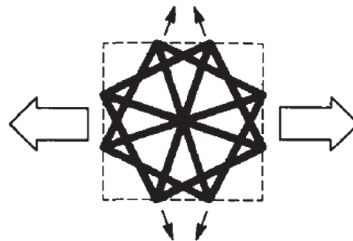


Figure 16. The tessellatable unit explained by Sigmund [44]

Rotating Polygons

In this structure the basic rotating units are polygons. The rotation doesn't occur along the centre of the polygon, but rather relative to each other, assuming that the polygons are rigid and that an external force is not reflected in an alteration of shape of the structure, but into rotation of the polygons.

Various structures using different polygons have been described, namely squares rectangles and triangles have been used. The square model has been used to describe the auxeticity observed in thomsonite and thus will be discussed later.

Rectangles are interesting, in that the Poisson ratio is dependent on a number of factors, which mainly arise due to the fact that rectangles having two sets of equal sides, resulting in two different major configurations of tessellated rectangles exhibiting a negative Poisson ratio under certain conditions [15].

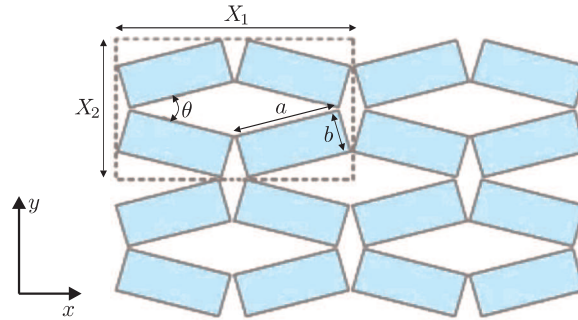


Figure 17. Rotating rectangles connected by equal sides [15]

One type of configuration involves one side of the rectangles being attached to the side of same length of another rectangle as shown in Figure 17.

Poisson ratio in this case depends on; the ratio of the unequal sides forming the rectangle ($a : b$ from figure above), and also on the angle between the longest sides of two triangles (θ). The pothorconformational arrangement is that of rectangles connected together with the unequal sides joined together, this result in a Poisson ratio of -1 irrespective of the previously mentioned parameters.

Triangles may also be used to build a structure with negative Poisson ratio (Figure 18). The mechanisms by which these materials respond to an external expansion in one direction is by hinging over the connections at the vertices of each triangle, resulting in an expansion of the system and thus a Poisson ratio of -1 .

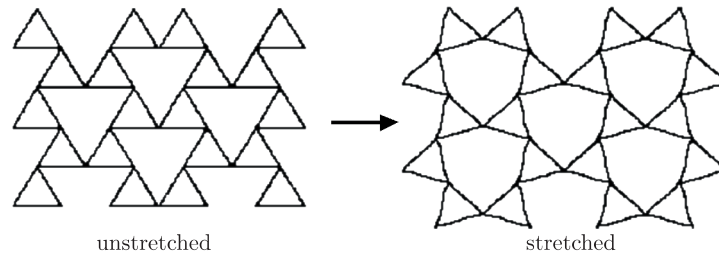


Figure 18. Rotating triangles upon application of stress [29]

This is exemplified at the molecular levels by means of polyphenylacetylene networks. As observed, these networks involve phenyl rings, connected through by means of acetylene chains, the nomenclature is thus polytriangles- n -yne, were n stands for the number of acetylene chains between each phenyl rings. In the case of polytriangles- n -yne networks with an $n > 2$, the structure is predicted to exhibit six negative Poisson ratios by molecular modelling simulations, and thus was termed as self expanding [45].

Foams also have been suggested to deform via a similar mechanism, As opposed to the re-entrant model, which suggest that during the compression/heating process the Y-shaped joints are inverted, the rotating triangles model suggest that

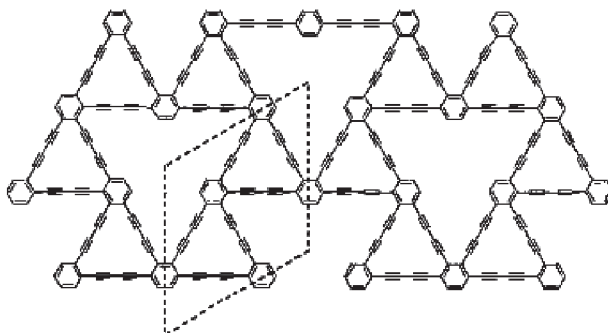


Figure 19. Structure of the polytriangle-2-yne [45]

the main deformation during compression occurs due to buckling of the ribs. This is because the relatively greater mass of material at the joints makes it difficult for them to be inverted so that these joints behave like rigid triangles and also deform through the rotating mechanism on loading, therefore explaining the auxetic behaviour in such foam [46].

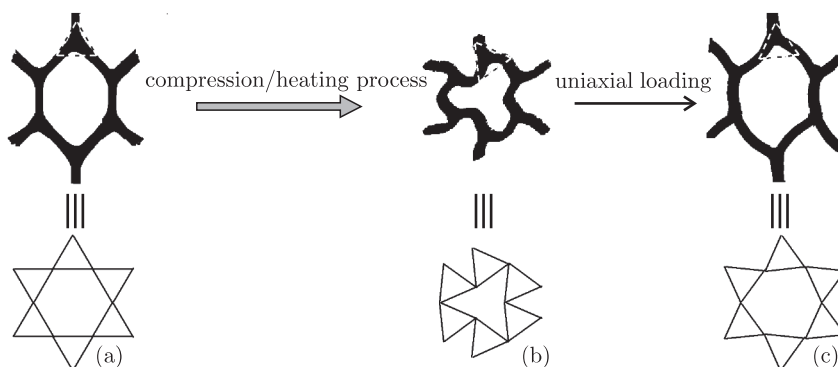


Figure 20. The conventional honeycomb (a), (b) the resulting honeycomb upon heating and (c) the auxetic honeycomb after stress, below; the idealised structures [46]

Rotating rods and helices

These were first described in the macro level as a concept, with rods joined together by another relatively flexible rod. Stress on this latter rod result in a rotation of the previous rigid rods, these will push the parallel chains and hence cause an expansion in the perpendicular direction – see Figure 21.

This model is used mainly to explain the mechanism behind auxeticity in a number of liquid crystalline polymers (LCPs), which are synthetically produced. The possibility that organic chemistry allows for manipulation of the bond formed in between structures, together with the relatively simple design of the general structure, was probably the main reason for the spur of interest in LCPs, with new auxetic designs being reported. [48]

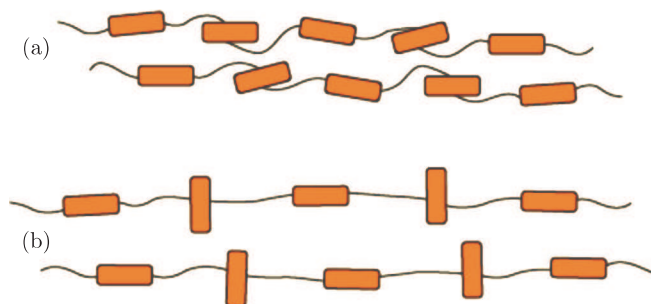


Figure 21. (a) When the chains are not under stress; (b) when the chains are stressed along the chain length [47]

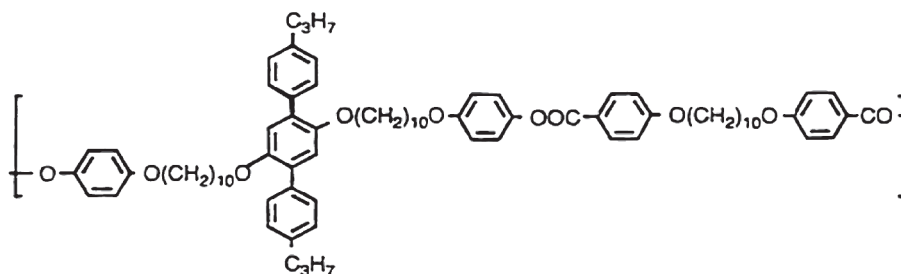


Figure 22. An example of a polymer having a rotatable part which results in auxeticity

The units alternate from rigid to flexible according to the designed polymer. The fact that the flexible unit must be able to rotate back into place dictates that the intramolecular interactions between parallel rods must not be high and thus composed only of weak e flexing rods, those rods which are laterally attached to the main rod must be of an adequate length such that a rotation of these rods would result in appreciable separation of the parallel rods running alongside, and hence a detectable expansion would be observed. Also the spacing of these laterally attached rods must be such that it allows for the lateral expansion of the whole rods parallel to it and not just local expansions. The lateral rods must also be attached to a flexible rod, in order to allow for the rotation to occur, i.e. allow for re-orientation to the parallel chain of the laterally attached rods after stress is removed [48].

2.1.1.5. Dilating auxetics

This mechanism was first developed indirectly for nuclear reactors in the 1950's in order to compensate for both the thermal expansions of the grapheme and steel sheets used, together with the possibilities of other destabilising affects such as earthquakes. [49–51]

In concept dilation mechanisms involve structures with bonds which are able to extend along an axis without the need for any other part of the system to rotate along an axis, hinge or flex. Put simple it is the elongation of a link within a geometrical unit. Perhaps the most quoted example in this case, and the easiest to comprehend is that by Rothenburg [52]. The basic unit is an auxetic triangle,

with a shock absorber within each side of the triangle, deforming in a piston-like fashion (see figure below), this unit may be used to construct larger structures, acting as a monomer.

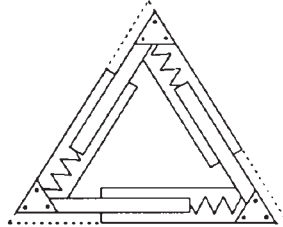


Figure 23. Auxetic triangular cell unit proposed by Rothenburg *et al.* showing the undeformed unit which can be used to build bigger auxetic structures (adapted from [52])

2.1.1.6. Multipods

This is a relatively new concept; it evolves an entanglement of pods connected together by means of a knot. The model used involves 6 pods, though different number of pods may be used, hence the name multipods, connected together by means of six- independent knots. These knots allow for the formation of lattices, and the interconnections result in each multipod joined with multipods from surrounding knots, the structure is preserved due to the mutual movement of the multipods, thus when pressure is applied, a complete contraction of the whole system results. In theory this structure can be constructed at the molecular level using rectangular lattices, proposed compounds include oxides, such as zinc and also carbon based backbones [53].

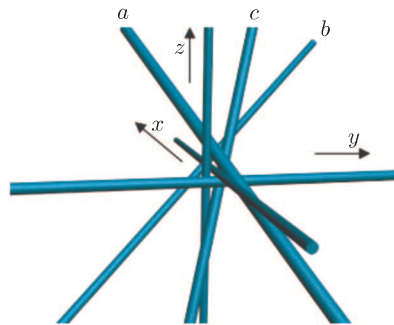


Figure 24. Figure showing the tessellatable 6-knot structure which would form rectangular lattices in order to produce an auxetic structure, the intertwining of pods is easily visible

2.1.2. Applications

Due to their particular properties, auxetic materials have a vast number of uses in industrial and conventional applications. One innovative application proposed by Mancini in 2005 was done in reference to electrical systems, which included the change in conductance properties of the system by altering specific

cell dimensions. Throughout the simulation Mancini and co-workers used C-Si-W, a granular metallic superconductor, and by application of tension were able to alternate the conductance properties, as it was found that specific angles and dimensions of the structure were related to critical super current [54].

The application of auxetic materials as smart filters is promising, due to the ability of changes in pore size, through application of stress. When considering nano and micro scale auxetics being used as filters, there pore size can be varied according to the size of particles allowed for separation; through the change in strain applied along the separating membrane which would be the auxetic material [55, 14]. This feature may be applied also to medical bandages, impregnated with medication, which is released upon swelling of the wound, since this cause tensile strain on the material. When the wound has healed and thus the swelling decreases, the amount of strain on the material decreases resulting in a pore size decrease and thus the amount of medication released is automatically regulated, according to requirement, acting as a smart filter [13].

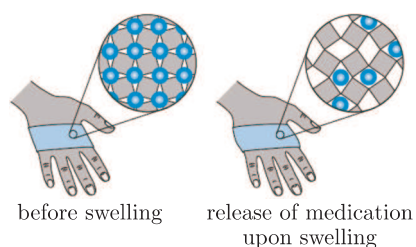


Figure 25. The auxetic smart bandage [13]

Auxetic foams have various characteristic properties which allow them to be used in car and aerospace industry. They have a relatively high indentation resistance, which means that they can be used in car seats, bumpers, safety equipment (crash helmets), bullet proof vests as well as aircraft nose cones. In response to bending forces, auxetic materials act very differently from conventional materials forming a dome shaped (synclastic) structure, as opposed to a saddle shaped (anticlastic) configuration demonstrated by conventional materials [13]. This particular property comes about due to the structure of re-entrant honey combs which allows densification on application of pressure through elastic collapse and is able to regain its shape after strain removal due to lack of rib failure on application of load [47]. By combining two composite fibre laminates with an auxetic foam core a strong curved surface can be generated and used in both cars and aeroplanes mainly due to its ability to resist impact and strains as previously noted. Light body armours as well as comfortable mattresses can be made of auxetic foams mainly due to their ability to adjust to the body curvatures accordingly.

Seat belts, rivets and gaskets can also be made out of materials with a negative Poisson's ratio. Conventional gaskets they tend to squeeze out when compressed while a negative material would expand upon compression therefore resulting in a better seal. On the same principles of gaskets, auxetic rivets would

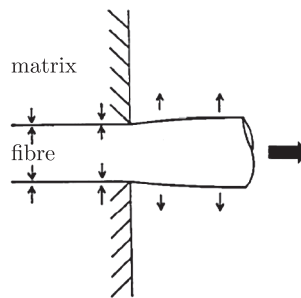


Figure 26. The apparent benefit of having an expansion in a rivet when pulled, resulting in a better hold [1]

be highly functional since upon being pulled out they would expand creating a better fit.

The same conceptual understanding may be applied to auxetic seat belts which upon the application of longitudinal pressure would increase in width therefore narrowing down the amount of pressure on the passenger in case of impact or sudden breaking [13].

Auxetic polymer matrices may be used in enhancing signal detection piezoelectric sensors in response to stress. When a piezoelectric sensor is placed in an auxetic polymer matrix, an applied vertical stress is translated to a horizontal one, thus amplifying it and generating a clearer signal. This has a potential application in ultrasonic medical systems and hydrophones [56].

2.2. Molecular modelling

Molecular modelling is a tool which allows researchers to model systems and observes them in a virtual environment, without the need of subjecting the system to any conventional experiments. It thus simulates these real systems as though in real life. The use of computing in research has increased significantly through the years and is becoming more important in research as; the increase of computational power available at a decreased cost allows for more realistic computational models to be simulated and conceived, together with the increase in costs for wet chemistry, due to various reasons, such as regulations, and cost of energy. The major drawback with simulations is that they are virtual, thus they are limited to the assumptions and knowledge we have of real life situations and the mathematical solutions we give to such situations may not represent the whole picture and thus never give the actual solution. The mathematical formulations used are usually collected in programs such as HyperChem, developed and produced by Hypercube, Inc., Cerius² and Materials Studio developed and produced by Accelrys. These programs allow for easier manipulation and building of structures, prior and after simulations, enhancing the manipulation of the results obtained and the ease of use, and combine different modules used in molecular modelling, allowing for easier excess to such sub-programs.

Molecular modelling is applicable to most scientific fields; the mathematical models used may vary from one field to another; for example different models are used to simulate organic and inorganic systems, in order to account for different and interatomic and inter/intra molecular interactions, also models used to study different features of a given system may be different due to different emphasis required for the study. Thus molecular modelling is a field of science on its own implemented in most fields nowadays.

The mathematical models used for molecular modelling may be regarded as divided into two main branches, that branch which considers quantum mechanical models as the basis for the energy expression of particles in the system, and another branch which bases its models on classical mechanics.

2.2.1. Quantum mechanical (QM) simulations

As the name implies, quantum mechanical simulations, use the Schrödinger's Wave function, with a number of approximations to generate the energy expression. This is a relatively accurate estimation of the system. The more assumptions used the lower the accuracy, but the faster the generation of expression. Thus, as it is common in molecular mechanics, the dilemma between the accuracy and computational time arises. This is usually overcome by due consideration of the system required for analysis, the accuracy required, available computational power and time available for the generation of the system. Models based on quantum mechanical simulations usually are more accurate in terms of atomic interactions, since more accurate mathematical expressions are used to simulate these, but the computational power required usually makes them less desirable for larger systems where such detailed analysis may not be required, such as was the case for this paper where an empirical model was used.

2.2.2. Force-field based models (empirical models)

These are different from QM simulations in that they completely ignore electrons. The bonds are represented by springs, bound to the nuclei, represented by balls, and the system is governed completely by Newton's laws of classical mechanics, which are much easier to compute than the quantum mechanical models. One of the first drawbacks is that the balls and springs in the system must be given certain properties, the balls are usually parameterised based on atomic masses and ionic radii, and thus an oxygen atom in water would be different than an oxygen atom in a solid, such as a zeolite, resulting in a number of atomic types. Data for springs is usually collected, either from quantum mechanical based simulations or from experimental data. This results in another drawback, that the force field being used must be parameterised for the system in question in order to allow for a real simulation of the system. Four different types of force-field may be identified;

Classical force-fields are relatively simple, rely heavily on the parameters available which are derived from quantum mechanical and/or experimental data and are mainly used for organic compounds. CVFF is an example of such a force field [57]

Rule-based force-fields these are relatively more transferable, compared to classical force-fields, in that they may be used for a wider range of chemical systems. The parameters are based on a number of atomic properties and include rules governing physical realities, such as atomic radii and electro-negativity, aiming to generate explicit force-field parameters. Examples include Universal 1.02 [58] and Dreiding 2.21 [59].

Second-generation force-fields focus on modelling the complex energy surface of a system; the small amount of parameters used in previous force-fields is not enough, and thus there parameters are extensive, with more analytical energy expressions including cross-terms, resulting in complex force-fields, most parameters, especially due to the complexity of extracting them experimentally; are derived from quantum mechanical simulations.

Specialised force-fields are used especially in areas where study of a particular system is required. They are parameterised to model specific systems, with amount of parameters being greatly reduced in some cases, resulting in highly specific force-fields. This results in a greater accuracy for smaller number of atoms, sacrificing transferability; for example the Burchart 1.01 [60], which contain parameter only for Si, Al, O and P, and thus can be used for systems containing exclusively only some or all of these atom types, such as zeolites, aluminosilicates and aluminophosphates.

2.2.3. Modules and molecular modelling software

Modules are usually used in modelling programs, in order to allow for long-existing algorithms to be incorporated within the main program. These algorithms may be available as stand-alone programs, such as GULP, but these usually are less user friendly, (for example GULP is a code-based program) [61] thus incorporation of these algorithms within molecular modelling programs, allow for easier inputting and transfer of data and use of these modules. Such modules include, amongst many, Forcite, Gulp and Discover, which allows for simulation of systems generating data from structures, such as the minimum energy conformations and mechanical properties of a system.

A variety of force-fields is available within these modules such as; CVFF (Consistent Valence Force-Field), PCFF (Polymer Consistent Force-Field) and COMPASS (Condensed-phase Optimised Molecular Potentials for Atomic Simulation Studies). The first two are more specific for organic or organic-like systems, containing parameters for atoms such as hydrogen, carbon, nitrogen, oxygen, sulfur, phosphorous, halogens, and silicon; and thus may be used for modelling of zeolites and like COMPASS have been validated for use in zeolite systems [62]. The COMPASS force-field is a more generalised force-field; it is the first *ab-initio* force-field to be parameterised and validated with the use of condensed-phase properties together with various *ab-initio* and empirical data, resulting in simultaneous and accurate; predictions of structural, conformational, vibrational and thermo-physical properties, under a wide range of conditions of temperature and pressure, for a broad range of systems, both in isolation and

condensed phase. COMPASS is especially used to model systems which contain both organic and inorganic molecules. Zeolitic systems have been modelled using COMPASS [63, 62, 13], and also systems such as alpha-cristabolite has been used to compare a number of force-fields and there adequacy to model siliceous zeolites, including COMPASS [64].

2.2.4. Molecular dynamic (MD) simulations

Minimisation simulations in static simulations model the system such that the atoms are placed in minima, according to conditions applied resulting in a minimised system, in other words a system having an energy minimum for those conditions. This situation is extremely ideal, since the system is described as static, lying in an energy minimum and not moving, as though at zero temperature, were no kinetic energy is available and no time or temperature variations occur.

In dynamic simulations, this idealised system is overcome by placing other considerations in the simulation. Time and temperature are some of the most important considerations involved. Dynamic simulations involve a system composed of a defined set of atoms with a potential energy, defined by a specific set of mathematical models, either Quantum mechanical or empirical may be used, for which the Newtonian laws of motions are solved over a period of time.

In real life situations; the total energy of the system is not conserved, a situation which is not possible in static simulations, simple integration of the Newtonian laws of classical mechanics allows the study of a system with constant energy surface, but will not give a good simulation of the real-life phenomena, were exchange of energy between the system and the outside occurs in one form or another. In order to account for phenomena like external pressure and heat exchange extended models are required in order to account for the change in the total energy of the system. These are termed ensembles.

2.2.4.1. Ensembles

These basically act as re-equilibrating systems in order to maintain the total energy of the system in check. Different statistical ensembles are available, depending on the variables (such as energy E , enthalpy $H(E+PV)$, number of particles N , pressure P , stress S , temperature T and volume V) are kept fixed, different statistical ensembles may be used on a system, from these statistical ensembles are generated and then a number of properties, including structural, energetic, and dynamic may be calculated over the ensemble generated by considering averages or fluctuations of the quantities over the ensemble. Ensembles are classified according to the factors used in order to maintain the system at a constant total energy and some of these include adiabatic and isothermal ensembles, such as the NVE (the microcanonical ensemble), the NVT (the canonical ensemble), NPH (constant-pressure, constant-enthalpy ensemble) and NPT (constant temperature, constant pressure ensemble).

The **NVE** ensemble is a Constant-energy, constant-volume ensemble or the microcanonical ensemble, it is obtained by solution of the standard Newton

equation without any temperature and pressure control. Thus energy is conserved in this adiabatic ensemble, and fluctuations observed are due to the rounding and truncation errors during integration processes.

NVT, also known as the canonical ensemble is a constant-temperature, constant-volume ensemble, obtained by control of the thermodynamic temperature; thus the variations in temperature are set and may be defined. It is ideal for use in conformational searches of models under vacuum and without any periodic boundaries, this result in reduced perturbations of trajectories due to the absence of coupling to a pressure bath.

NPH, constant-pressure, constant-enthalpy ensemble; it is the analogue of the constant-volume, constant-energy ensemble, (NVE), where the size of the unit cell is allowed to vary [65]. This allows for the enthalpy, H ; the sum of E and PV , to be kept fixed at constant pressure without the need of temperature control.

NPT is known as the constant temperature, constant pressure ensemble, allows for control on temperature and pressure as well as stress. The pressure is adjusted by adjustment in volume and the allowing unit cell vectors to change, hence the size, and in some variants the shape, of the unit cell change. Such a method applies only for periodic systems. Control of pressure may be brought about by the Berendsen, Andersen, or Parrinello-Rahman method, the first two allow only for the size and not the shape of the unit cell to change, and thus only the Parrinello-Rahman method can be used for changes in stress, since it allows for both shape and volume changes. Thus this ensemble (NPT) together with this barostat (Parrinello-Rahman method) method will be used for this paper since stress changes are studied. For temperature control any method suited for the system may be used, but the temperature scaling method cannot be used since it is not truly isothermal. This system is usually used when correct pressure, volume, and densities are important in the simulation, and due to the ability of the method to cause changes in the shape of the system, and thus allowing stress along particular axial directions, it is ideal for simulations involving the study of stress-strain and related mechanical properties on specific systems.

The statistical ensemble of NPT thus uses two main concepts for maintenance of a constant pressure and temperature; the thermostat and barostat.

2.2.4.2. Timestep

Another factor which one must consider in dynamic simulation is the major variable itself; time. The frequency of recording the simulation, and thus the frequency of calculating all of the system properties and the parameters mentioned above are of major importance. This parameter is termed the integration time step Δt . Typical time steps range from 0.5 to 2 fs. As one may easily intuit, the larger the time step the less computational power required for a simulation with a given time period, but the larger the time step the less calculations are made on the systems, and thus the less the system is representative of reality. Also the reduced calculations may result in instability of the system or inaccuracy in integration processes. The lower the time steps the easier one may note any

changes in the system such as, shape, structure and energy changes, reducing also the chances of actually overlooking changes within the system at particular time intervals. Considerations on the choice of time step usually involve the highest frequency motion being considered within the system, the faster the this motion, the shorter the time step should be, since these should not be overlooked, and must be sampled at least 8 to 10 times in order to ascertain the assumption, that the velocities and accelerations are constant over the time step used, this is known as the Verlet assumption. Depending on the study undertaken, having a shorter time-step allow for more samples of fast motion for a given atom or bond to be worked out, and thus give a more representative picture of the actual interactions occurring, since more samples of this motion are taken for each step, thus having more statistically significant results and also making the system less prone to instability. Thus the choice of time step is greatly dependant on both the system under study and the scope of the study. For example, organic systems, if they contain hydrogen to carbon bond, whose stretching frequency lies within the 10^{-14} s (10 fs), must be of 0.5–1.0 fs.

2.2.4.3. Temperature control in MD simulations

The approach used for controlling the system's temperature varies. Temperature is an important factor in dynamic simulations, the distribution of atomic velocities within a system are highly dependent on the temperature of the system, which are related through the Maxwell-Boltzmann equation;

$$f(v)dv = \left(\frac{m}{2\pi kt} \right)^{\frac{3}{2}} e^{-\frac{mv_x^2}{2kt}} dv_x \quad (2)$$

The role of these thermostats is basically to absorb the excess wave energy generated through vibrations and movement, in absence of such methods, the propagation of energy through the system would result in erroneous final trajectories, due to the reflection of this excess energy from the system's boundaries. Different systems and different studies may require different temperature controls, depending on importance and affects of the excess energy present within the system on both the system and the studied properties; thus, due consideration of the particular thermostat method used is required to attain the desired quality of results. Some particular thermostat methods used include:

1. The Velocity Scale method (direct velocity scaling)
2. The Andersen method
3. The Berendsen Method
4. The Nose method

The **Velocity Scale method** involves the maintenance of temperature within a given range of a target temperature, by scaling the atomic velocities accordingly when drift of the average temperature out of the specified range occurs, this results in a quick equilibrium and is thus used to control the kinetic temperature of the system, such a method is extremely unrealistic and is not used in order to study true temperature affects.

The **Andersen** method generates randomised velocities for atoms at a pre-defined collision frequency. In this way, as with the Nose, the thermodynamic and not the kinetic temperature are kept constant, which is required for true temperature control. On the other hand the control by randomisation results in discontinuous trajectories, and in unsmooth velocity changes, as opposed to the Nose.

In the **Berendsen** method, the rate of heat transfer between the system and temperature bath may be controlled, applications are usually limited to small scale systems, having small surface areas, this is important in order to maintain a constant temperature. It is most effective in maintaining temperatures at early stages of dynamics, but will fail near ends of simulation, with an increase in the system's temperature. [66]

The **Nose** method is possibly one of the most realistic models, [67–69] it is a method involving true canonical ensembles both in coordinate states and in momentum space. This method is basically a simplified re-formulation of Hoover [70], which eliminates time scaling resulting in real time trajectories at specific time intervals. The idea behind this method is an additional fictitious degree of freedom with a mass, Q , representing the interactions between the heat bath and the system. The choice of mass thus will dictate the thermostat capability and hence the ability for the method to maintain the system at the desired temperature, according to the actual mass and the degrees of freedom within the system. This method gives a realistic approach to temperature control, and allows continuity in trajectories of atoms, making it adequate for correlation studies.

2.2.4.4. Pressure control in MD simulations

It is important in order to maintain a constant pressure in a system. Pressure is calculated through the use of the virial theorem [71]. Like temperature pressure is a thermodynamic quantity and is strictly speaking, meaningful only at equilibrium. Thermodynamic pressure, temperature volume and internal virial can be related in the following way:

$$PV = Nk_bT + \frac{2}{3}\langle W \rangle \quad (3)$$

As with temperature the pressure and stress control mechanism must produce the correct statistical ensemble; and hence the probability of occurrence for a certain configuration will obey the laws of statistical mechanics. Various barostats are available including the Andersen, Berendsen, and Parinello-Rahman method.

In the **Andersen** method, the volume of the cell is allowed to change as in the Parinello-Rahman method, but its shape is preserved by allowing the cell to change isotropically. Thus this method is not useful for stress tests, but is useful for liquid simulations, since the system could become quite elongated in the absence of restoring forces if the shape of the cell is allowed to change, a constant shape also make dynamics analysis easier [65].

The **Berendsen** method couples the system to a pressure bath thus maintaining the pressure at a certain target, similar to the system used for temperature, this coupling strength is determined; both by the compressibility of the system and by a relaxation time constant. This method changes the cell uniformly such that the size of the cell is changed but not its shape [66]. Therefore for simulations such as phase transitions of crystals, where both the cell size and shape are expected to change, this method is not appropriate.

The **Parinello-Rahman** method [72] allows simulation of a molecular system under externally applied stress or pressure. This is especially useful for studying stress-strain relationship of materials and is possible since both the shape and the volume of the cell are allowed to change, so that the internal stress of the system can match the externally applied stress. The Lagrangians of the system are modified such that a term representing the kinetic energy of the cell depends on a user defined mass-like parameter \mathbf{W} . An elastic energy term $p\Omega$ is related to the pressure and volume or the stress and strain of the system. The equations of motion for the atoms and cell factors can be derived from this Lagrangian; (the motion of the cell vectors, which determines the cell shape and size, is driven by the difference between the target and internal stress);

$$L = \frac{1}{2} \sum_{i=1}^N m_i \dot{\mathbf{s}}_i' \mathbf{G} \dot{\mathbf{s}} - \sum_{i=1}^N \sum_{j>i}^N \emptyset(r_{ij}) + \frac{1}{2} \mathbf{W} \text{Tr} \dot{h}' \dot{h} - p\Omega \quad (4)$$

(Where h is equal to $(a.b.c)$ is the cell vector matrix and $\mathbf{G} = h'h$, $r_i = h s_i$, \emptyset is the interaction potential, and Ω is the volume of the cell. The dots above some symbols indicate time derivatives and the primes indicate matrix transposition. Tr is the trace of a matrix.) In order to simulate stress the elastic term $p\Omega$ is replaced by;

$$p(\Omega - \Omega_0) + \Omega_0 \text{Tr}(\mathbf{S} - p)\varepsilon \quad (5)$$

(Where \mathbf{S} is the applied stress, Ω_0 is the initial volume and ε is the strain.)

2.3. Zeolite structures

2.3.1. Introduction

A zeolite is a mineral, defined as a crystalline substance whose structure is characterised by the framework of linked tetrahedral, each consisting of four oxygen atoms surrounding a cation, the framework contains open cavities forming channels and cages, usually occupied by water molecules and extra-framework cations, which are exchangeable and channels are large enough for the passage of guest species. Dehydration of the hydrated phase may be brought about by heating to temperatures usually not exceeding 400°C, and is usually reversible. Framework structure may be interrupted with OH, or F groups, these occupy an apex of the tetrahedron and cannot be shared by adjacent tetrahedra. [73] The three-dimensional framework structure is usually composed of SiO_4 and AlO_4 tetrahedra, linked to each other by sharing the oxygens, resulting in the interconnections of cages and channels, the hollow structures, which contain water

molecules and ions, which are mainly composed of alkali and/or alkaline earth cations. Other elements may be observed in some zeolites, such as phosphorous and beryllium and the extent of replacement of these elements may be even up to 50% of the original silicon and aluminium content [74].

The word zeolite means boil stone [73], the first zeolites were described over 200 year ago. Initially they were thought to be formed under volcanic reactions, including reactions between lava flows and hydrothermal springs, they were found in sources of sedimentary rock, and near volcanic active areas. The presence of zeolites near the surface of the earth implies that their formation is not under extreme conditions. Zeolites are produced synthetically as well, and of interest is the production of highly siliceous zeolites which are more desirable, especially in applications such as filters and adsorbents of pollution. [75]

2.3.2. Auxeticity of zeolites with focus on THO

A number of zeolites have been found, or have been predicted to, show auxetic characteristics in at least one of their planes. Such zeolites include THO, NAT and EDI all of which are grouped together, due to the similarity in their framework (Figure 27). In particular, Grima *et al.* had predicted through static force-field based simulation that these siliceous forms of these zeolite frameworks are all predicted to exhibit auxetic behaviour in their (001) plane. This was the first time that negative Poisson ratio had been attributed to zeolites [14].

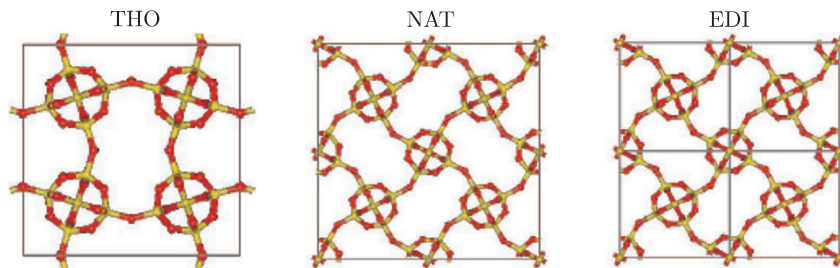


Figure 27. The single unit cell of THO, NAT and EDI in the (001) plane [12]

In Grima *et al.*'s early work on zeolites [14], the zeolites were arranged in order to produce ideal structures, by removing all of the interstitial cations and water molecules, and the framework was an all-silica model, (i.e. all of the aluminium ions were replaced by silicon). Siliceous zeolites such as these have been studied extensively via molecular modelling, especially with focus on their auxetic properties. Although the frameworks for different types of siliceous zeolites are different, the basic elements present are the same; silicon and oxygen. Also the bonding in the framework structure is the same for these siliceous zeolites, thus studies regarding the choice of parameters for one zeolite may be easily extrapolated to another zeolite, although the more similar the framework the more valid is this assumption. A major work on a similar system to zeolites, α -cristobalite, was done to show the suitability of empirical models to simulate

such a system, and it was shown that amongst various force-fields, COMPASS and Burchart were suitable for simulation *n* of such and similar systems [64].

Grima's study in 2000 was performed using a variety of force-fields, mainly the Burchart, BKS, Universal, and CVFF force-fields, a number of idealised zeolites were modelled in order to identify their Poisson's ratios. This study had shown that the hypothetical all silica equivalents of these systems are predicted to have a negative Poisson's ratio in the range of -0.64 to -0.34 [45], in the (001) plane, depending on which force-field was used. A mechanism was also proposed for the deformation of these structures upon stress so as to show a negative Poisson ratio.

In this mechanism geometry transformations that result when these systems are uniaxially mechanically loaded are explainable through a 'rotating polygon' mechanism. For example, as illustrated in Figure 28, thomsonite (THO), has framework geometry in the (001) plane, which may be described as being made up of squares joined together at the vertices.

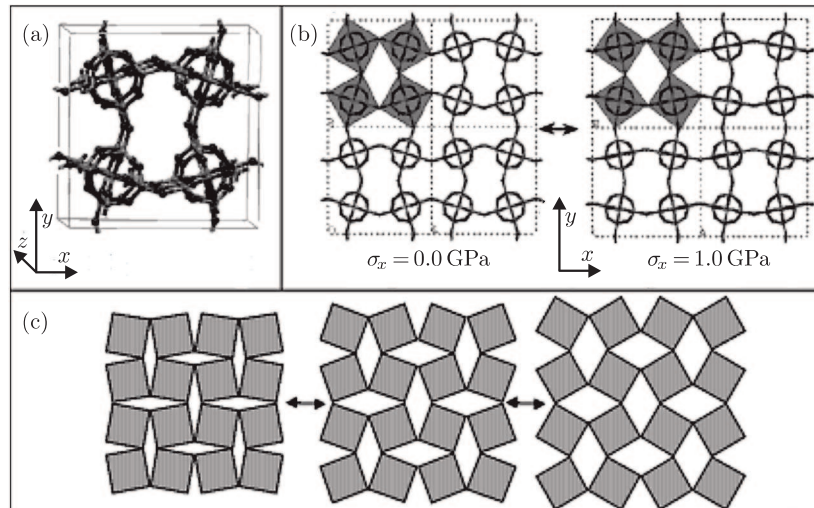


Figure 28. (a) The structure of THO in the (001) plane (b) minimum energy conformations at different stresses for THO with the squares highlighted; (c) the highly idealised 'rotating rigid squares' mechanism which affords Poisson's ratios of -1 [14]

Similar to the system described previously on rotating rectangles, the squares in THO are assumed to be rigid, and joined together by hinges along which rotation may occur. Thus in order to show auxeticity the squares need only to rotate relative to each other. The original macro-scale model is basically made up of squares, connected at the vertices together by hinges. Under idealised conditions, were the system is able to deform as a rotating polygon under stress, this system exhibit a negative Poisson ratio of -1 [14].

Further work by Grima showed that THO does in fact exhibit a negative Poisson ratio, but not of -1 , as predicted by the rigid square model, but about -0.6 in the (010) plane, according to molecular simulations [46]. This led Grima

et al. to propose a modified explanation of the mechanisms interplaying within the system. The major mechanism is, as described by Grima [45], that of rotating squares, but these projected squares are in fact semi-rigid. This mechanism is essentially similar to the rigid squares, in that rotation of these projected squares, with respect to each other occurs, but the force applied during application of stress or strain is not completely transferred to rotating of the squares, but some deformation of the framework making up the squares also occur. The degree of deformation is dependent on the stiffness of the internal framework, and results in changes in lengths of the diagonals making up the projected squares, rotation of these diagonals over each other, and changes in the angles between the sides of the squares. This deformation, though results in parallelograms and is not that large, compared to the major mechanism occurring within the system that of the rotation of the projected parallelograms over the Si-O-Si hinges [12].

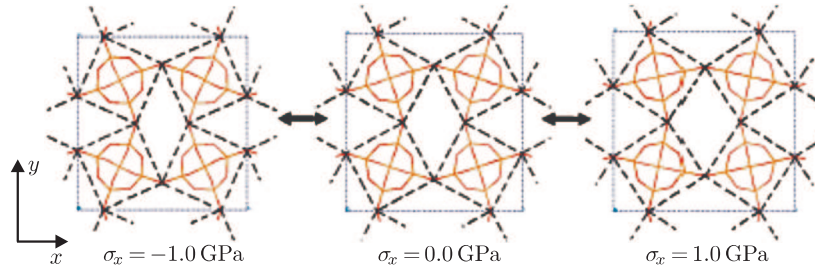


Figure 29. THO in the (001) plane at different stresses along the x axis

Other interesting studies has been carried out on similar systems, such as NAT, which has been studied more extensively than THO, both experimentally [20] and *via* molecular modelling [14, 15, 12, 16–19]. The Poisson ratio of the real system of NAT, has been determined to be negative ($\nu = -0.12$) in the (001) plane at $\pm 45^\circ$ off axes, [16] thus establishing in both of these studies, that even for the real system, it is negative [20, 16] and that molecular simulations are in fact able to predict such mechanical properties.

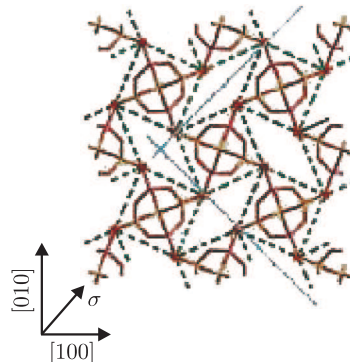


Figure 30. The crystal structure of NAT in the (001) plane with interstitial cations [16]

NAT, EDI and THO have been studied in terms of their auxeticity at non-ambient conditions of hydrostatic pressure. It was shown that under such conditions their auxetic nature is enhanced especially at positive external hydrostatic pressures approximately of 2–8% of the bulk modulus [19]

2.3.3. Uses of zeolites and general properties

The framework of zeolites, as described above, possesses a number of cavities and this results in properties, such as reversible water-adsorption and the ability for some of the zeolites to be used as metal cation exchangers. Some zeolites, such as chabazite, are able to adsorb molecules with ability to hydrogen bond, including some organic molecules such as short-chain alcohols, example methanol, ethanol and even formic acid vapour.

These properties to adsorb molecules and exchange cations have led to zeolites being applied as adsorbents and desiccants such as for separation and purification of air, especially zeolites with intermediate silicon to aluminium ratio [76].

Another benefit that the open framework gives rise to is the high internal surface area, which makes zeolites ideal to act as catalyst for petroleum refining and ion exchanging. Synthetic zeolites are preferred in industry, since natural zeolites are of lower purity and less uniform, thus resulting in products which are less reliable [76].

Of more interest to the properties studied in this paper is their application as molecular sieves and cationic exchangers. These applications arise both from the open framework and also the ability to balance the cations present within the framework, due to the charges present on the alumina and silica forming the framework. The molecular-sized pores allow for the compound to act as a molecular sieve, to which the auxetic properties of the structure infer particular advantages due to the ability to arrange the pore size, causing specific sized-pores under specific stress, and hence specifying the pore size of the molecular sieve without need for physical change of the sieve.

2.4. Scope of this paper

All of the work done on zeolites; in regards to their negative Poisson ratio, have been mainly produced *via* molecular modelling simulations, using static models. These simulations are able to give the mechanical properties of a structure, but consider relatively ideal situations, without considering factors, such as the natural vibrations of the system over a period of time as a result of a non-zero temperature. Static simulations are thus sometimes regarded with a degree of scepticism, as to regards the actual effects of the studied parameters on real-life systems. Dynamic simulations; on the other hand, are more realistic since factors, like temperature and time, are included as variables in the simulation, resulting in a nearer-to-life simulation, as opposed to static simulations, where only the structure at an energy minimum is given. Thus this study aims at establishing the degree of representation able to be produced via static simulations

when compared to dynamic simulations on zeolites and similar systems. This will be done using the idealised siliceous equivalent of the THO framework as a representative model, henceforth referred to as THO-SI. This framework was chosen in view of the fact that the early works on zeolites had been focussed on this system as it has the advantage of exhibiting maximum negative Poisson's ratio for loading on axis. Furthermore, due to its simple composition (the effect of the interstitial cations and water molecules are not included), this THO-SI system is very easy to model from a computational point of view.

This work on THO-SI will be conducted through force-field based molecular dynamics (MD) simulations using the COMPASS force-field which as discussed later, is suitable for modelling of such systems. However, since all previous studies had been conducted using other simpler force-fields, this MD study will be preceded by a statics study using the same force-field.

3. Static simulation of THO

3.1. Introduction

As stated before, THO and similar structures, such as NAT and EDI have already been studied for their negative Poisson ratio by means of static molecular simulations. Specific force-fields are available, such as Burchart, which are designed to simulate zeolites specifically, and thus these are the most commonly used in studies of such systems [14, 15, 12, 16–18]. In this paper, the dynamic simulation will be executed via the Discover module in the Materials Studio program; this limited the choice of force-fields to three, the PCFF, CVFF and COMPASS. Amongst these three force-fields two have been used in simulations of such siliceous zeolites, the CVFF and COMPASS. The choice of COMPASS over CVFF was due to the fact that the COMPASS force-field is a newer force-field than the CVFF and studies have shown that it is highly suitable for modelling of siliceous frameworks (e.g. α -cristobalite [64]). More recently, the COMPASS has been used in a number of studies simulating siliceous zeolites similar to THO, such as NAT, and THO itself [19]. This shows further that it is an adequate force-field for simulating the siliceous-THO system. In view of all this, the work in this paper will be conducted using the COMPASS force-field.

These published studies suggest that although different force-fields show the same basic result, that THO and similar zeolites have auxeticity in their (001) plane, the magnitude of this predicted auxeticity may vary between one force-field and another [14, 15, 12, 16–19]. For example in the study by Grima and co-workers in 2000, it was predicted that the value of ν_{xy} for THO (001) plane varied between -0.64 to -0.35 , depending on which force-field was used. In this section, an attempt will be made to perform a static study on THO using the COMPASS force-field. This will not only be beneficial as it may provide additional confirmation regarding the auxeticity of THO, but, more importantly as it will enable a direct comparison between the static and dynamic properties of THO which will also be simulated using the COMPASS force-field. Thus any possible

variations within values of Poisson ratios and other mechanical properties as simulated by statics and dynamics studies would be attributable to the difference in the choice of simulation, between a static and dynamic model, and not due to differences in other parameters, such as force-field used.

In view of all this, this section presents the methodology used and results of static simulations performed using the COMPASS force-field in an attempt to re-predict the Poisson's ratios the deformation mechanism. This results are comparable to the values of Poisson ratio and deformation mechanism in literature in order to ascertain that the chosen force-field is adequate for the THO system and is able to describe the mechanism occurring under stress in a manner which is comparable to the literature available. This is so as to ensure that the results obtained here may act as a link between available literature done via static simulations and the further work provided in this paper on dynamic simulations and hence allow for comparison between the dynamic and static models of the system; thus enabling discussion on the adequacy for choice of static or dynamic simulations.

3.2. Simulation of the minimum energy conformations and mechanical properties for mechanical loading in the x direction

3.2.1. Methodology

Simulations of the static properties presented in this section were performed using the Cerius² package (Accelrys Inc.) running on an Octane 2 SGI workstation. The simulation was driven via the graphical interface available within the program.

Simulations were performed on the siliceous equivalent of the THO zeolite framework, i.e. taking the THO aluminium-silica derivative, without any water and intra-framework cations with the modification that the aluminium atoms were replaced with silicon atoms. The original THO framework used was the one available in the Cerius² database which was imported from X-Ray experimental data [77]. Note that henceforth, this SiO₂ equivalent will be simply referred to as THO-SI.

Although, as previous work has shown, a single unit cell is sufficient to effectively simulate the mechanical properties of a zeolite like THO-SI through statics simulations [78], in order to extract more easily the parameters required, such as atomic coordinates, the unit cell used was enlarged to $2 \times 2 \times 1$ and converted to a super cell, so as to be able to chose a unit cell-equivalent with no atoms on the border of the system, facilitating the manipulation for extraction of results. This also has the beneficial effect that a more realistic system is modelled (in general, the larger the unit cell, the more realistic the system is) without affecting by any detectable means whatsoever the computational time for obtaining the results. All symmetry constrains were then removed by 'converting' the symmetry from *Pncn* to P1 symmetry. Note that P1 is the minimal symmetry restrain that can be used in such simulations, ideal for simulations of mechanical

properties, particularly the Poisson's ratio, as it ensures that simulated properties are not artefacts of the symmetry. The structure used for the simulation is illustrated in Figure 31.

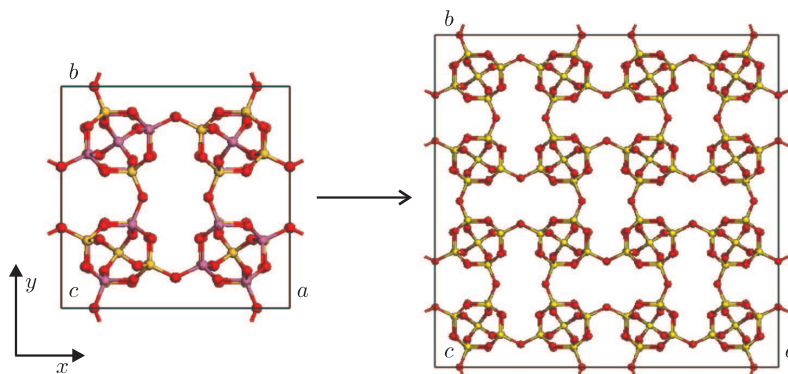


Figure 31. The initial unit cell and the super cell created by this unit cell (purple atoms represent Aluminium, yellow silicone and red oxygen), shown in the (001) plane

In the simulations, the crystals were aligned in such a way that their [001] direction was always parallel to the z global direction, the [010] direction was contained to lie in the yz plane whilst the [100] direction was free to adopt any orientation.

All structures were saved as a `.msi` files. This file format is ideal since it not only contains all the lattice parameters and atomic coordinates, but also in its header, it records the lattice vectors of the unit cell, namely:

$$\begin{aligned} a &= a_1i + a_2j + a_3k \\ b &= 0i + b_2j + b_3k \\ c &= 0i + 0j + c_3k \end{aligned} \quad (6)$$

From these, the projections of the unit cell in the x , y and z directions may be read directly and are given by a_1 , b_2 and c_3 respectively.

An energy expression was then set up using the COMPASS force-field as implemented in Cerius² version 4.1 [79]. (This force-field was chosen for the reasons mentioned earlier.) All parameters and settings were as defined in the force-field with the exception of the summation method for the non-bond interactions for both the van der Walls (vdW) and Coulombic terms which were summed using the Ewald Summation method [80] with a fine quality.

The systems were then 'minimised' (i.e. the geometry of the systems were optimised to conformations having lower energy) at the conditions of zero external stress using the SMART minimiser as implemented in Cerius² v. 4.1. The SMART minimiser is a compound minimiser which implements different minimisation procedures according to the requirements of the system during the minimisation. The SMART minimiser commences the minimisations with the Steepest descend

method and then when a particular convergence is reached, variants of the Newton-Raphsen method are applied.

Minimisations were performed to high convergence criteria as defined by Cerius² which include an RMS gradient less than 0.001 kcal mol⁻¹Å⁻¹. The system was minimised successfully within less than 5000 steps and was completed in less than a minute.

The minimum energy conformations at various levels of uniaxial stress in the x direction, namely $\sigma_x = 1.0$ GPa, -0.5 GPa, 0.0 GPa (already obtained), $+0.5$ GPa and $+1.0$ GPa, were then obtained. Note that in attempt to avoid discontinuities, the systems at 0.5 GPa and -0.5 GPa stress were obtained by re-minimising the systems with zero load directly whilst the systems with a -1.0 and 1.0 GPa of stress were simulated from the -0.5 and 0.5 GPa systems respectively.

The projections of the unit cell in the x , y and z directions at each stress σ_x were then extracted and used to calculate the engineering strains e in these directions as follows:

$$e = \frac{\Delta L}{L} \quad (7)$$

where ΔL is the change in length and L is the original length (i.e. length at zero stress) [81].

Since the Young's modulus is considered as the ratio of the uniaxial stress (in GPa) to the uniaxial strain, the Young's modulus in x , E_x , was found by plotting a scatter graph of strain e_x against stress σ_x , taking the best straight line with zero intercept. The value of Young's modulus, E_x , in GPa, is then obtained by inverting the gradient of the line, i.e. $E_x = m^{-1}$ with m being the gradient.

The Poisson ratio ν_{xy} in the (001) plane for loading in the x direction was then worked out by plotting a scatter graph of strain e_y against strain e_x , taking the best straight line with zero intercept. The value of Poisson ratio ν_{xy} is then obtained by taking the negative of the gradient m , i.e. $\nu_{xy} = -m$. Similarly, the Poisson's ratio ν_{xz} in the (010) plane for loading in the x direction was obtained from the negative of the gradient of a strain e_z against strain e_x graph.

3.2.2. Results and discussion

The results of these simulations are summarised in Figures 32–34 and Tables 1–2.

In particular, images of the projections in the (001), (100) and (010) planes of the minimised conformation of THO-SI at zero stress are shown in Figure 32 where it is compared with the equivalent projections of the THO framework as obtained from X-Ray crystallography data. These images clearly show the similarity in the framework of these two different systems, which may result in similarity of their mechanical properties. It also confirms that the COMPASS force-field can model the structure of THO-SI well.

Also shown are images of the projections of the crystal in the (001) plane (see Figure 33), i.e. as viewed down the z -axis, under different stresses σ_x in the x direction. A comparison of the structures under different stresses shows

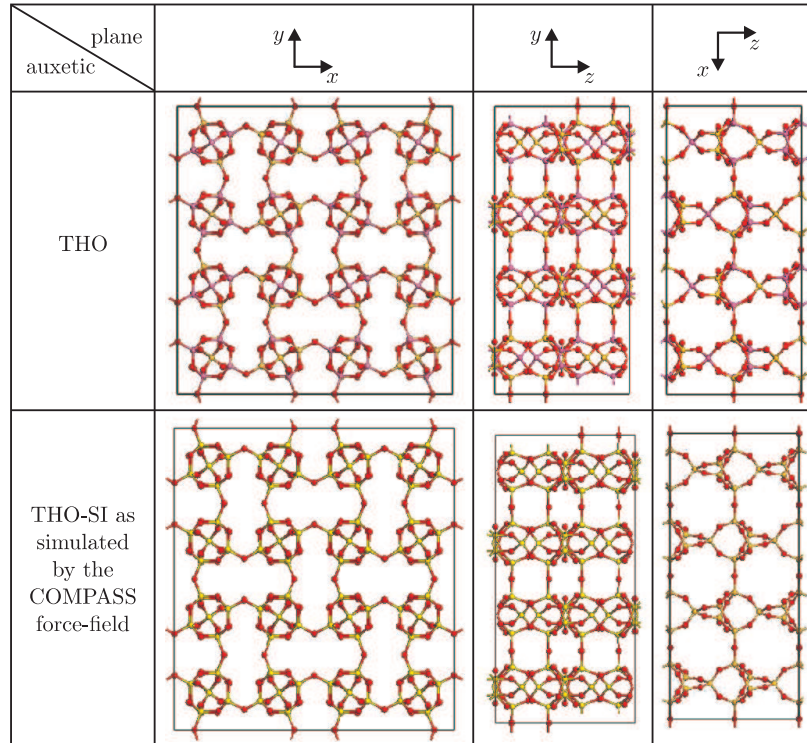


Figure 32. Comparison of the differences between THO and siliceous THO after minimisation at the (001), (100) and (010) planes

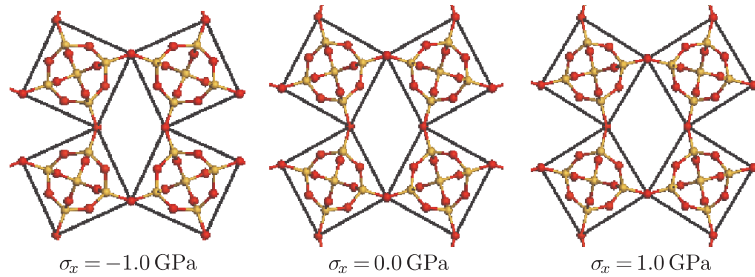


Figure 33. Comparison in the adjustment of the (001) plane of a single unit cell to different stresses in the x direction

a difference in the placements of the hypothetical units described as ‘squares’, these are observed to rotate with respect to each other when subjected to loads along the x direction. This results in ‘opening up’ of the structure when the load is increased (see Figure 33) since the angle between these squares may be observed to increase as the load along the x direction is increased. This rotation of the ‘projected squares’ results in a negative Poisson’s ratio, a property which is evident from a visual inspection of these systems and from the measurements of the unit cell projections in the x and y directions (Table 1) and strain-strain graphs (Figure 34b).

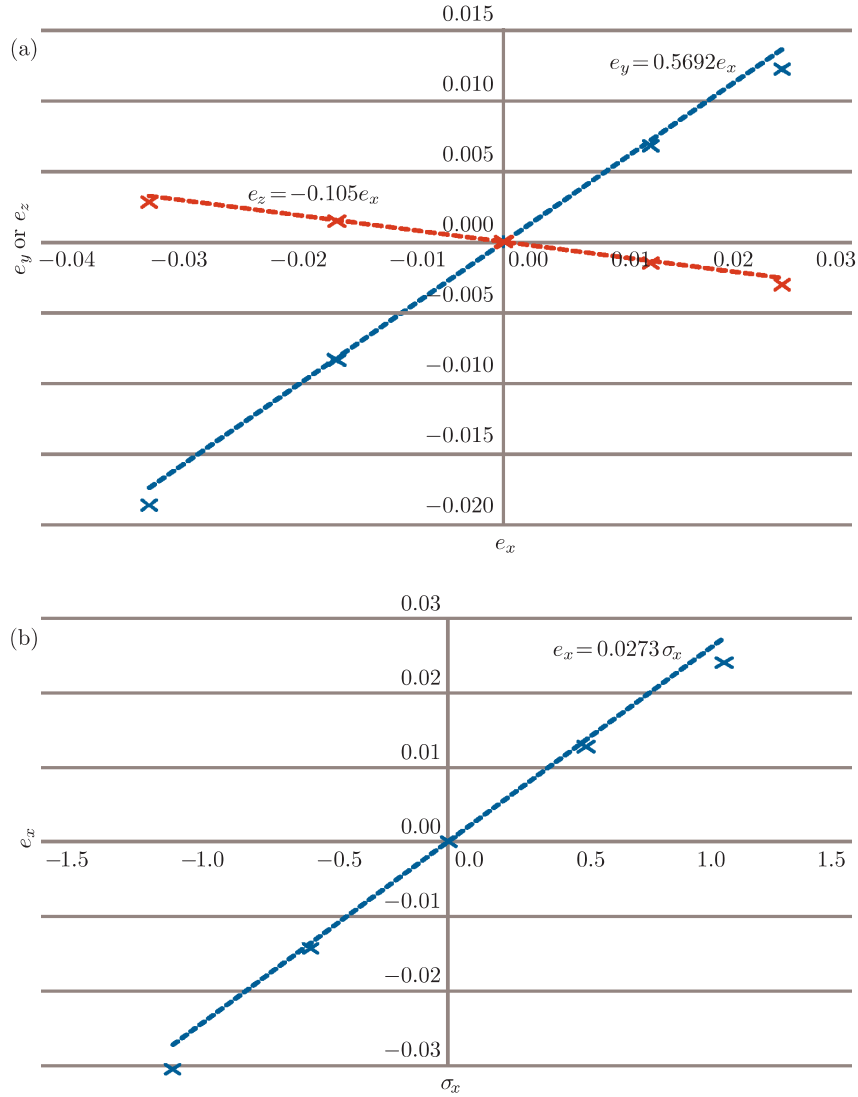


Figure 34. (a) Plot of e_y vs. e_x (blue) and e_z vs. e_x (red) where ν_{xy} and $\nu_{xz} = -m$ for respective plots; (b) plot of e_x against ρ_x (GPa; blue) where $E_x = m^{-1}$

In fact, Table 1 which shows the lattice projections along the different axes at different stresses, suggests that there is a general increase in the length of the unit cell along the x direction, as stress is increased; this is as expected from any material (The Young's modulus is normally positive). On the other hand, the length of the lattice in the y direction is also increasing as the stress and strain is increased along the x direction. Also as compression is applied along the x -axis, a decrease in length along both y and x axis is observed, implying an evident auxeticity. In contrast to this, the changes in length along z , compared to the changes in y and x are relatively small.

Table 1. Table showing; the projections of the unit cells (Å) along the x , y and z directions at different stresses (GPa) applied along the x axis of the $2 \times 2 \times 1$ unit (note that the projections of the $1 \times 1 \times 1$ units may be obtained by $x/2$, $y/2$ and z respectively; the strain on the structure along the axis at different stresses along the x axis is also shown)

σ_x (GPa)	Projection of the Unit cells in the x , y and z directions (Å)			Strain along axis		
	$x = a_1$	$y = b_2$	$z = c_3$	e_x	e_y	e_z
-1.0	25.91	26.23	12.89	-0.0306	-0.0186	0.0028
-0.5	26.34	26.50	12.87	-0.0144	-0.0084	0.0014
0.0	26.72	26.73	12.85	0.0000	0.0000	0.0000
0.5	27.06	26.91	12.83	0.0127	0.0068	-0.0015
1.0	27.36	27.05	12.81	0.0240	0.0122	-0.0030

Table 2. Comparison of the values for Young’s Modulus (GPa) and Poisson’s ratio for THO as obtained from different force-fields; ^a [14], ^b [12]

Force-field used	E_x (GPa)	ν_{xy}	ν_{xz}
COMPASS	36.63	-0.57	0.11
Burchart ^a	32.6	-0.64	-
Catlow ^a	41.8	-0.63	-
BKS ^b	-	-0.55	-
CVFF ^b	-	-0.56	-
Universal ^b	-	-0.35	-

All this is in accordance with what was observed by Grima *et al.* in similar studies using different force-fields. The fact that this new study confirms this mechanism is very significant as it provides additional evidence to the hypothesis being proposed that THO type frameworks exhibit negative Poisson’s ratio which may be explained through a ‘rotating squares’ mechanism. Furthermore, if one looks at the actual Young’s modulus and Poisson’s ratios simulated using this static study (see Table 2), one notes that values predicted compare well with the published ones using different force-field and suggest that for loading in the x direction, the Poisson ratio in the xy plane is negative (-0.57) and that for xz plane is positive (+0.11). This is very important since when more than one force-field predicts the same trend in results; then there is more evidence that what is being simulated is truly manifested in the real material and is not simply an artefact of the force-field used.

3.3. Analysis of the deformation mechanism

This section presents a study aimed at elucidating the deformation mechanism that results in the predicted NPR in THO-SI using the COMPASS force-field. This mechanism is compared to earlier published work by Grima and co-workers in their paper ‘Auxetic behaviour from rotating semi-rigid units’ [12].

Grima's mechanism projects the THO-Si framework as squares with oxygen atoms at their vertices. Grima proposed that if these oxygen atoms act as 'hinges', then the squares would be able to rotate. In fact, the results of Grima *et al.*'s simulations suggest that when the THO-SI framework was loaded in tension, the projected squares behave like 'semi-rigid squares' which primarily rotate relative to each other and, to a lesser extent, deform by becoming more parallelogram-like. A mechanical model to describe such deformations was also proposed.

The data obtained was thus manipulated as to project similar structures on the system as presented in the paper. Previous studies have also shown that it is enough to consider the equivalent of a single unit cell since all of the other squares behave similarly, to these [82].

3.3.1. Methodology

The minimised conformations obtained in the previous sections were analysed in such a way that the projected dimensions in the (001) plane of four projected 'squares' could be measured. Here it should be noted that previous studies have also shown that it is enough to consider the equivalent of a single unit cell since all of the other squares behave similarly, to these [82]. In view of these, only the data related to the four squares highlighted in Figure 32 a was extracted. (The smallest unit cell of THO contains four squares.)

This analysis was performed by extracting the x and y coordinates of the hinge oxygen atoms related to these four squares and use these to calculate the various lengths and angles associated with them. All the variables and parameters measured are defined in Figure 35 c, which variable parameters arising from deformation of these squares by the aforementioned mechanism, were also compared to those found in literature. Note that for this analysis, the atoms which correspond to the corners of the polygons were given a representative letter, which was comparable with the representative labelling provided in the Grima *et al.* paper. Note that in the paper, the actual squares used are a tessellate of the one used in this paper, although due to symmetry, this will not have an effect on the analysis.

3.3.2. Results and discussion

The actual lengths and angles associated with the system at 0 stress are shown in table. These results clearly show that the system is indeed describable in terms of connected squares since:

1. All the lengths AB , BC , CD and DA in the system are equal to each other (4.93).
2. All the angles ABC , BCD , CDA and DAB are equal to 90.00° ;
3. The diagonals AC and BD of the squares are all equal to each other (6.97)
4. The angles between the diagonals are equal to 90.04° .

This confirms that the analysis in terms of rotating semi-rigid squares can indeed be performed for the THO-SI system as simulated by the COMPASS force-

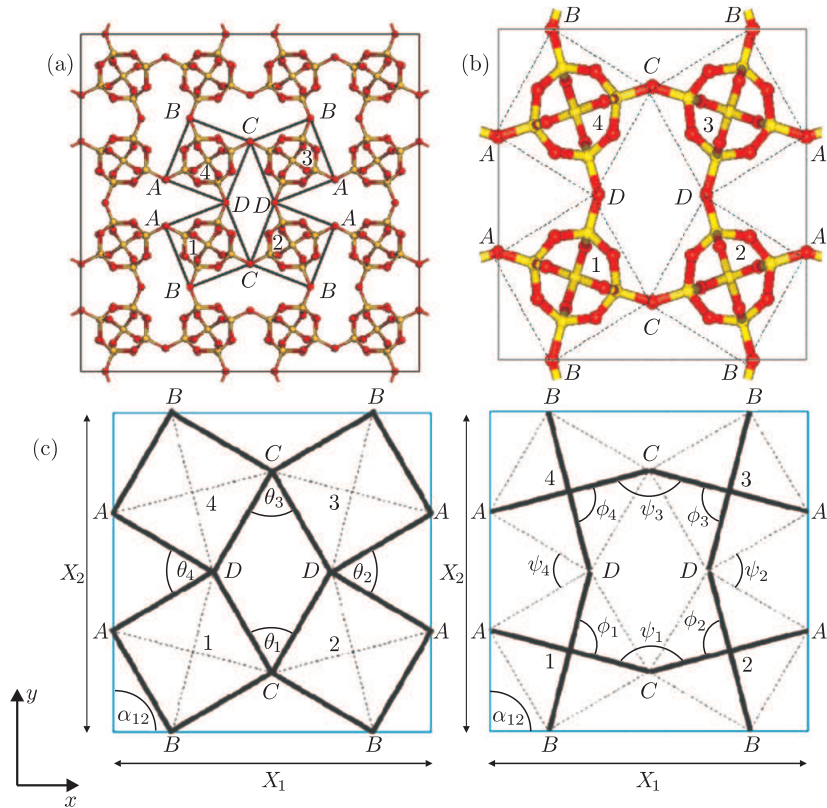


Figure 35. (a) The system simulated, with the chosen squares highlighted; (b) the systems as depicted in the paper by Grima [12]; (c) figure of the squares under study depicting the diagonals, AC and BD , and the angles; internal (ϕ) and external (θ) and (Ψ) which combines both the opening and closing of the squares, defined by θ , and the change in angle between the adjoining diagonals and the sides of the squares partially defined by ϕ (adopted from [12])

field. This data also suggests that the smaller angle between the squares, θ' is initially 56.63. This value compares well with that observed in real THO.

Also shown is a table showing changes in the parameters defined above compared to the values reported in the paper by Grima *et al.* (obtained using the Burchart force-field). Note that since the results by Grima *et al.* and the ones obtained corresponded to the deformations when the systems are equivalent to the systems being subjected to a stress of 1 GPa, then since the simulated moduli are slightly different ($E_x = 32.6$ GPa in Grima's study, $E_x = 36.6$ GPa present study); for a proper comparison it would be more appropriate to compare Grima's result to a modulated form of the present results where, the present results are scaled by $(36.6/32.6)$. These modulated values are also shown in Table 4.

In general, these results show that the same trend is followed by any variable parameter within the system. In particular, it is confirmed that the major deformations are as a result of the changes in the angles between the 'squares'. A detailed comparison suggests that the changes in angles as simulated by the

Table 3. Actual lengths and angles associated with the system at zero stress

	Square (n)	1	2	3	4
Sides	$A_n B_n$	4.93	4.93	4.93	4.93
	$B_n C_n$	4.93	4.93	4.93	4.93
	$C_n D_n$	4.93	4.93	4.93	4.93
	$A_n D_n$	4.93	4.93	4.93	4.93
Diagonals	$A_n C_n$	6.97	6.97	6.97	6.97
	$B_n D_n$	6.97	6.97	6.97	6.97
Angles	$D_n A_n B_n$	90.00	90.00	90.00	90.00
	$A_n B_n C_n$	90.00	90.00	90.00	90.00
	$B_n C_n D_n$	90.00	90.00	90.00	90.00
	$C_n D_n A_n$	90.00	90.00	90.00	90.00
Angle between diagonals	ϕ_n	90.04	90.04	90.04	90.04
Angles between squares	θ_n	56.63	56.63	56.63	56.63
	ψ_n	146.59	146.66	146.66	146.59

COMPASS force-field are slightly less than those predicted by Grima's earlier study (modulated values are 8.345° or 7.048° , compared with 9.442° found in the literature). Also interesting is the fact that the COMPASS force-field predicts that the change in the angle changes are not all equal to each other, a property which was also observed in an earlier study on natrolite³ with its standard composition using the Burchart and CVFF force-fields.

It may also be observed that the percentage change of length in both diagonals, AC and BD , show the same trends in both simulations, in that diagonal AC shows a small percentage increase, while BD show a small percentage decrease. This further shows that the square formation is slightly deformed, since the diagonals are no longer equivalent in length. This was also observed by Grima in their paper [83] which analysis the deformations in NAT where it is proposed that the squares in NAT are in reality slightly parallelogrammic. Apart from a change in length of the diagonals, comparing angle ϕ , also shows that the diagonals rotate over each other, such that the near 90° , angle present at zero stress, changes by a 0.372° , in the COMPASS simulation, which compares relatively well with the 0.352° change observed in other study.

The angles between the sides of the squares also follow the same trends in both studies. Of interest is that change in one angle is mapped with nearly the same magnitude by the change in another opposing angle, for both studies. In other words, an increase in angle ABC is mapped by a decrease in angle BCD , for any specific square, which is of the same magnitude. It should be noted that a larger change is observed in these internal angles for the COMPASS force-field

3. Natrolite (NAT) is a zeolite which is very similar in structure to THO.

Table 4. Comparison of the gradients of plots of % changes in lengths and actual changes in angles ($^{\circ}$) against applied stress (GPa) in x from work done by Grima [12] and modulated work done in this paper by the COMPASS force-field for THO-SI (*note that values for θ presented as part of the work by Grima for squares 2 was reported as -9.442° , in the paper, here it is reported as 9.442° instead, since this is an error – Grima personal communication)

	% fractional changes in length								Changes in the internal angles of the squares ($^{\circ}$)				Changes in angles between two quadrilaterals ($^{\circ}$)	
	n	$A_n B_n$	$B_n C_n$	$C_n D_n$	$D_n A_n$	$A_n C_n$	$B_n D_n$	$A_n B_n C_n$	$B_n C_n D_n$	$C_n D_n A_n$	$D_n A_n B_n$	ϕ_n	θ_n^*	Ψ_n
COMPASS modulated	1	0.030	0.678	0.030	0.678	0.919	-0.212	0.648	-0.648	0.648	-0.648	-0.372	8.345	8.069
	2	0.030	0.678	0.030	0.678	0.919	-0.212	0.648	-0.648	0.648	-0.648	-0.372	7.048	7.327
	3	0.030	0.678	0.030	0.678	0.919	-0.212	0.649	-0.649	0.649	-0.649	-0.372	8.345	8.069
	4	0.030	0.678	0.030	0.678	0.919	-0.212	0.649	-0.649	0.649	-0.649	-0.372	7.048	7.326
Grima [12]	1	-0.150	0.464	-0.150	0.465	0.613	-0.299	0.523	-0.523	0.522	-0.523	-0.352	9.442	9.272
	2	-0.150	0.464	-0.150	0.464	0.613	-0.299	0.523	-0.523	0.523	-0.523	-0.352	9.442	8.568
	3	-0.150	0.464	-0.150	0.464	0.613	-0.299	0.523	-0.523	0.523	-0.523	-0.352	9.442	9.272
	4	-0.150	0.464	-0.150	0.464	0.613	-0.299	0.523	-0.523	0.523	-0.523	-0.352	9.442	8.568

when compared to the earlier work by Grima *et al.* which confirms the hypothesis that the squares as simulated by COMPASS are less rigid than those simulated by Burchart. In other words, the COMPASS force-field simulate the oxygen atoms, acting as vertices of the squares, as being bonded less rigidly and thus more deformations may be observed in this system, than that simulated by Grima, this is also reflected by the larger change in the diagonal AC .

The main discrepancy that is observed is in the changes in the sides of the ‘squares’. In their study, Grima *et al.* [12] identify two sets of sides, those which decrease in size, AB and CD , and those which show a percentage increase in size, BC and DA . Grima *et al.* also noted that the actual decrease in BC and DA was considerably smaller than the increase in the other sides, AB and CD . The simulations presented here suggest that although there is an agreement in the sense that the set of opposite sides BC and DA change more than the other set AB and CD , there is disagreement in the ways that the sides AB and CD change. In fact, the results presented in Table 4 show that with the COMPASS force-field, both sets of sides actually show a percentage increase, as opposed to the study by Grima, where there was a percentage decrease. It should be noted, though that this increase is small, only 0.030% (Grima *et al.*’s decrease was -0.15%). On the other hand, the sides which in the paper show an overall percentage increase, BC and DA , in the results presented here also show an increase, but the increase is larger; 0.678% as opposed to 0.464%, observed in this same set of sides, by Grima *et al.* Here it is interesting to note that the difference between the two force-fields is a relatively constant, i.e. with the COMPASS force-field, all the four sides of the squares increase by around 0.180–0.214% when compared to the Burchart. Furthermore, comparing the percentage changes between the two sets for the same force-field; the system modelled by COMPASS shows a 0.648%, while a 0.614% difference is observed for the system modelled by Burchart.

Before we conclude it is important to note that that the main conclusion of these results is not that there is overall force-field dependence of how the squares deform (although to a lesser extent there is), but that rotation mechanism is indeed the main deformation mechanism taking place. In fact, it should be highlighted that when comparing these percentage changes in lengths related to each square, one should consider them in the light of the percentage change in the cell projections. Referring to Figure 35c, X_1 and X_2 as simulated by the Burchart varied by 3.04% and 1.95% respectively, while for the study by COMPASS, they varied by 2.73% and 1.54% respectively (modulated to 3.06% and 1.72% respectively, when one multiplies by the 1.12 correction factor). In other words, the percentage changes in the lengths of the sides of squares or the lengths of diagonals is a much smaller change than the changes observed in the overall cell projection. Similarly, the angle changes related to angles of an individual square are observed to change much less than the angles between the squares, i.e. the deformation in the squares, for both studies, are much less than the deformations of the overall unit cells or the changes in the angles between the projected ‘squares’.

All this is very significant as it confirms, to a first approximation the deformation mechanism is indeed as that of rotating ‘squares’ (or more precisely rotating ‘semi-rigid’ squares which become parallelogramic) when they are subjected to a uniaxially stress in x a direction of maximum auxeticity. The fact that the COMPASS force-field can capture this major mode of deformation, and also the less dominant modes, particularly the fact that the squares are predicted to become parallelogramic, a property which was also found in NAT having its experimental composition, [82], confirms the suitability of the COMPASS force-field, for studying this framework.

3.4. Conclusion

From this section it may be concluded that:

1. The COMPASS force-field is adequately parametrised to model THO-SI as it can predict the correct shape of framework and can predict mechanical properties which compare well to those found in the literature;
2. The statics study using the COMPASS force-field can reproduce the predicted auxeticity for THO-SI;
3. The COMPASS force-field is able to reproduce the prediction that the major mechanism that of rotating squares. It is also able to predict the less dominant mechanisms, such as that of deforming squares. In fact, only slight discrepancies are present between parameters predicted by different force-fields.

In view of all this it may be concluded that the COMPASS force-field is an adequate force-field to model such and similar systems, like NAT. Also due to the slight discrepancies between the force-fields, for comparison of dynamic and static simulations, it is preferable that the data generated by the COMPASS is used so as to eliminate any discrepancies due to the use of different force-field.

4. Dynamic simulations

4.1. Introduction

As noted in the literature review, dynamic simulations are considered as being more realistic than static simulations due to their ability to simulate systems at realistic temperatures and to simulate the behaviour of systems over a period of time (ps range). Before this work no study was made regarding the auxeticity of zeolites *via* dynamic simulations and this section will attempt to rectify this lacuna by performing dynamics simulations on the siliceous THO empty framework THO-SI. This study is essential so as to obtain evidence as whether or not static simulations performed in the previous section and by other workers are indeed realistic. Also, it will propose a suitable methodology for simulations of stress on THO-SI and similar systems.

In an attempt of comparison, various factors will be discussed; ranging from the similarity or trends between parameters, differences between their magnitudes, together with the ability to determine the mechanisms by which auxeticity occurs.

Also other factors, such as time for running of simulations and extraction and manipulation of parameters will be considered, and also the difference in the amount of data offered by the two different methods.

It is expected that the dynamic simulations will show a greater variation within the results obtained for the different parameters, for various reasons; including the fact that a number of structures will be present from which an average structure is worked out, all of these structures are valid and represent the some of the possible changes of geometry, occurring within the system at different instances of that situation, which is the scope of dynamic runs, and the factor which makes them more realistic.

This section will first develop the methodology to be used to perform the molecular dynamics simulations at 300 K at various values of stress in the x direction and to extract the data so as to obtain measurements related to the projections of the unit cell in the x , y and z dimension at the various stresses and use these to calculate the mechanical properties. This will be followed by a full analysis aimed at obtaining the average dimensions related to the connected squares model as performed in the previous section so as to identify the deformation mechanism through dynamics simulations. The results obtained will be compared with the statics work.

4.2. MD simulations at various stresses and simulation of the mechanical properties

The aim of this section is to develop the methodology to be used to perform the molecular dynamics simulations on THO-SI for performing simulations at various values of stress in the x direction. This will include the actual dynamics simulation, the extraction of the data so as to obtain measurements related to the projections of the unit cell in the x , y and z dimension, as well as calculation of the mechanical properties which will be compared to the statics work.

4.2.1. Methodology

The dynamics simulations

The simulations were executed through the Materials Studio (MS) package running on an Intel Xeon-64 bit architecture, Quad Core 2.6GHz CPU computer having 24GB DDR3 RAM and a 64-Bit XP operating system installed. Materials Studio (MS) can execute computations in parallel and thus the 4 CPU's were used. MD simulations are available within MS through two modules namely MS-Discover and MS-Forcite. However, it is only MS-Discover which have the ability of running simulations at different values of uniaxial stress rather than pressure and thus the simulations will be performed using MS-Discover.

MS-Discover is supplied with a number of force-field including the COMPASS force-field which in the previous was established as being valid for simulations of the siliceous THO system. The first steps, that of obtaining the structure, arranging its size, its symmetry and minimising it at a value of zero stress, were done as described in the previous section, but with the graphical interface provided by

the Materials Studio program. The choice of lattice structure for running dynamic simulations was first by a $1 \times 1 \times 1$ unit cell, followed by a $2 \times 2 \times 1$ and then by a $3 \times 3 \times 3$ system. The choice for such sizes was developed after comparison of results, which will be discussed here.

The parameters for choice, other than those required similar to static simulations include mainly; the choice of system size, the time step, the ensemble to be used, the barostat and thermostat to be used, temperature at which the system is maintained and the time the simulation was allowed to run.

The time-step used was that of 2 fs for the larger systems, when the smaller system, of $1 \times 1 \times 1$ unit cell was tested, it was impractical to choose a large time step, since such a system is less stable and would have collapsed easier, had the same time-step been chosen. The value of a 2 fs time step was chosen on the basis of a study [84], where a similar system was simulated. The system was that of cristobalite, this system, similar to our system, is composed of silicon and oxygen atoms bonded together. As stated earlier, the choice of time step is dependent on the vibrational frequencies of components within the system, and since these systems are made up of the same elements, having the same order of bonds, together with the fact that the 2 fs lies within the range conventionally used for most systems, it may be relatively adequate to use the 2 fs time step as an adequate value, which is further confirmed when one considers that the atoms involved within the system, are fairly large and bonded intrinsically in a relatively rigid framework.

The time the simulation was allowed to run was chosen on the basis of the time equilibration was achieved and whether the amount of frames available after equilibration was enough to be statistically significant. For the $2 \times 2 \times 1$ and $3 \times 3 \times 3$ system, the Dynamics time was set at 1000 ps, and since for the $1 \times 1 \times 1$ system, the timestep was of 1 fs, the dynamic time chosen was 500 ps, since had no equilibration been reached yet, most probably the system would not equilibrate.

A detailed literature review of ensemble, barostat and thermostat were already discussed in sections, 2.2.4.1, 2.2.4.3 and 2.2.4.4 respectively. The basic conclusions from that review are that the NPT ensemble is the ensemble of choice, since it allows for a system with a constant temperature and pressure. The barostat identified for use was the Parinello-Rahman method; [72] since this is the only method which allows for a change in stress. The Nose method [67–69] was used as the thermostat, because it gives a control of temperature which results in fine trajectories for atoms, as opposed to the Andersen method [65]. and is also good for fairly long simulations with relatively large systems, as opposed to the Berendsen method [66], which is suitable for short simulations and smaller systems.

The temperature of choice was of 300 K, which is a realistic temperature, in which real systems are normally exposed to, thus making the simulation more realistic than the static, which simulated the system at 0 K. The pressure was set at 0 GPa for the first simulation, but it varied depending on the different stresses

applied on the system. Stress was varied only along the x direction, with a range of -1.0 to 1.0 GPa at 0.5 unit intervals, (i.e. the stresses under which each system was simulated were; -1.0 , -0.5 , 0.0 , 0.5 and 1.0 GPa).

The trajectory was saved in full every 50 steps, i.e. the structures as well as the velocities were saved every 50 steps. This enables one to extract $250,000/50 = 5,000$ frames from the simulation at periodic time intervals which are meant to give a representative sample of the properties of the system. Note that this setting was chosen so as to optimise the data saved : disk space ratio.

The simulation was thus run. Simulation times ranged from few hours to nearly one week, depending on the size of the system.

Data extraction

(i) Extraction of the potential energy and temperature profile of the simulation

MS discover has the facility to generate potential energy *vs.* simulation time, kinetic energy *vs.* simulation time and temperature *vs.* simulation time automatically. Thus these plots were generated through the software.

(ii) Extraction of structures in a periodic manner from the simulation

The frames saved during the run were exported from the trajectory as `.msi` files so as to make them easier to manipulate, this was done by means of a Perl script. Perl was chosen since this language is supported by Materials Studio (MS) and could thus be run from within the program. These frames contained all the information on the system, ranging from lattice parameters to atomic coordinates within the system, both of which were required for this paper.

A typical Perl script used was⁴:

```
#!/perl
use strict;
use MaterialsScript qw(:all);
my $doc = $Documents{"THO_minimised.txt"};
my $interval = 10;
my $start_frame = 2000;
my $number_of_frames = $doc->Trajectory->NumFrames;
for (my $frame_counter = $start_frame;
     $frame_counter <= $number_of_frames;
     $frame_counter = $frame_counter + $interval) {
    $doc->Trajectory->CurrentFrame = $frame_counter;
    $doc->Export("C:\3_3_3\THO_0.0\THO_333_0.0".
               "_".$frame_counter.".msi");
}
```

This script requires definition of two parameters of interest, the starting frame for extraction and the interval at which each frame had to be extracted. The starting frame was chosen by observing the temperature and potential energy graphs build up by MS during the simulation and identifying the place from which equilibration of the system had occurred, for the larger system, $3 \times 3 \times 3$ it was at

4. This Perl script was supplied by Ruben Gatt.

2000. The smaller the interval the more representations of the data and thus the more significant the statistics, it was taken at ten, resulting in a set of 301 frames, this was considered as enough especially for the larger system, where variation within the data was found to be small (see discussion).

(iii) *Extraction of the projections of the unit cell in the x , y and z dimensions and calculation of the mechanical properties*

As seen from the script, the files were saved in the `.msi` format, these were then further manipulated by another stand-alone program, written in Microsoft Visual C#⁵, which allowed extraction of specific lines within each saved trajectory file, and saving them in one text file, this allowed for easier manipulation of data from each file, found at a specific line within each file, such data included the lattice cell parameters and specific atomic coordinates and IDs.

This data was converted to `.xls` format. The lattice parameters were averaged out and the mechanical properties for each system calculated from them.

4.2.2. Results and discussion

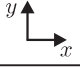
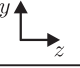

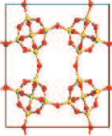
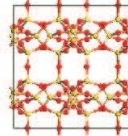
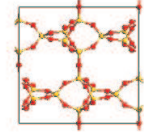
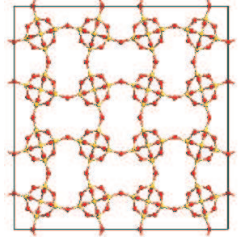
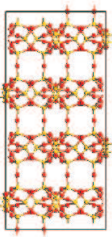
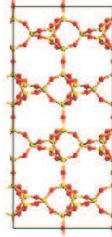
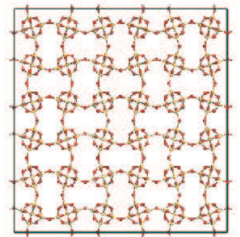
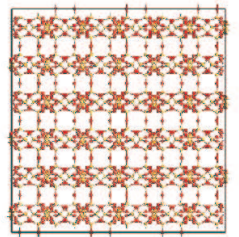
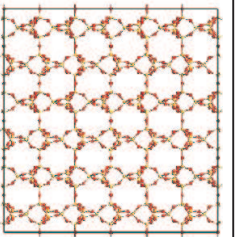
The structures of the different lattice sizes in the different planes, obtained after minimisation are shown in Table 5. Animations of the frames in there (001) plane for the different lattice sizes, at the different stresses of -1.0 , 0.0 and 1.0 GPa are supplied in the supplementary information in electronic format. Also shown are representative plots ($\sigma = 0$ GPa) of the potential energy and temperature variation within the system during the simulation (Figures 36–37). In order to compare quantitatively the difference in the mechanical properties of each system, the Young's modulus and Poisson ratio were worked out (see Figures 38–39 respectively). The standard deviation of the lattice parameters at -1.0 , 0.0 and 1.0 GPa for all axis are shown in Table 6. Followed by a comparison of the mechanical properties, E_x , v_{xy} and v_{xz} , between the three systems used for dynamics and the static simulation (Table 7).

From the animations provided as an electronic format, one may evidently see the deformations occurring in the system with a $1 \times 1 \times 1$ lattice size; the slightly less deformed $2 \times 2 \times 2$ and the more realistic behaviour from a relatively rigid framework expected from system such as THO, observed in the $3 \times 3 \times 3$ unit size, especially at the two extremities of stress. Observation of the whole trajectory, results in a much better comprehension of deformations occurring within the smaller lattice sizes and the general mechanisms exhibited by the different systems upon application of stress.

Stabilisation of the structure during the run is also observed in terms of the variation of temperature and potential and kinetic energies of the system. In all cases, these graphs typically initiate with a large variation of the parameter and stabilize off as the run proceeds. The faster the stabilisation at the beginning and the less variation of points about a mean, at the end of the run, imply a more stable system. Data to be used for work on the system was extracted

5. This program was supplied by Michael Ciantar.

Table 5. Showing the different lattice size of the systems studied in the different planes after minimisation

plane unit cell			
1×1×1			
2×2×1			
3×3×3			

from frames lying after the phase where temperature and energy of the system has stabilised with that of the temperature bath. This shows the importance of such graphs, apart from giving a good indication of the stability of the system along the dynamic simulation, and at what time the system stabilised, they also indicate the appropriate time from which sampling of frames should take place.

For the first two unit cell sizes, temperature was not observed to equilibrate sufficiently, and thus as one may observe, the temperature variation of the system was fairly large, this is most evident in the $2 \times 2 \times 1$ unit cell size. The temperature deviation for $1 \times 1 \times 1$ varied within a range of 200 K and for $2 \times 2 \times 1$ a range variation of 300 K was observed, as opposed to the 50 K variation range observed in the $3 \times 3 \times 3$ unit cell size. Temperature variation is important especially for determination of atomic loci, since the atomic velocity, and hence their movement, are dependent partially on temperature, via the Boltzmann distribution; and hence studies which require specific atomic coordinates, need as much as possible few variations of the system's temperature.

The temperature variation is lower for the $1 \times 1 \times 1$ system, than the $2 \times 2 \times 1$ though it is evident, from observation of the trajectory files, that the movement within the atoms is much more irregular in the $1 \times 1 \times 1$ system. It is of interest, however to observe the standard deviation of the unit cell parameters,

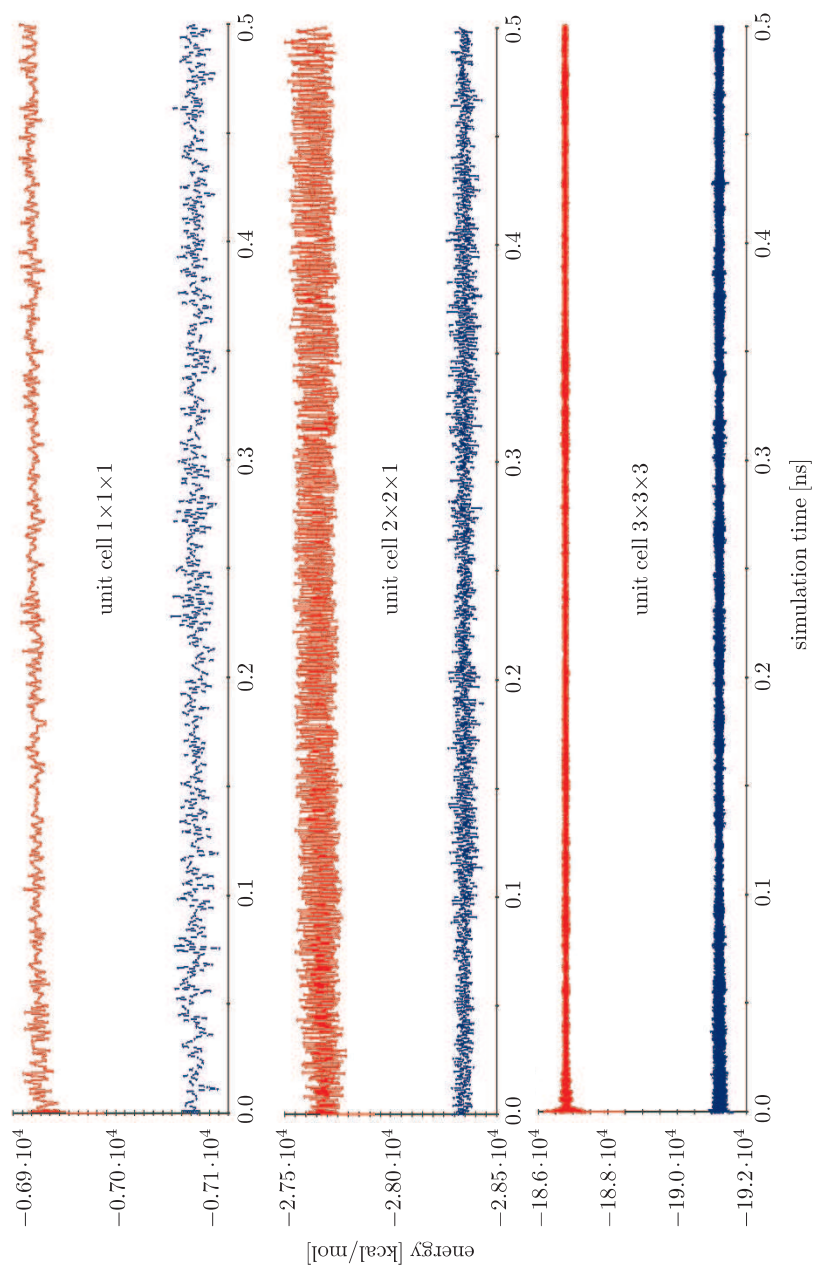


Figure 36. Plots of the potential energy and non bond energy vs. simulation time

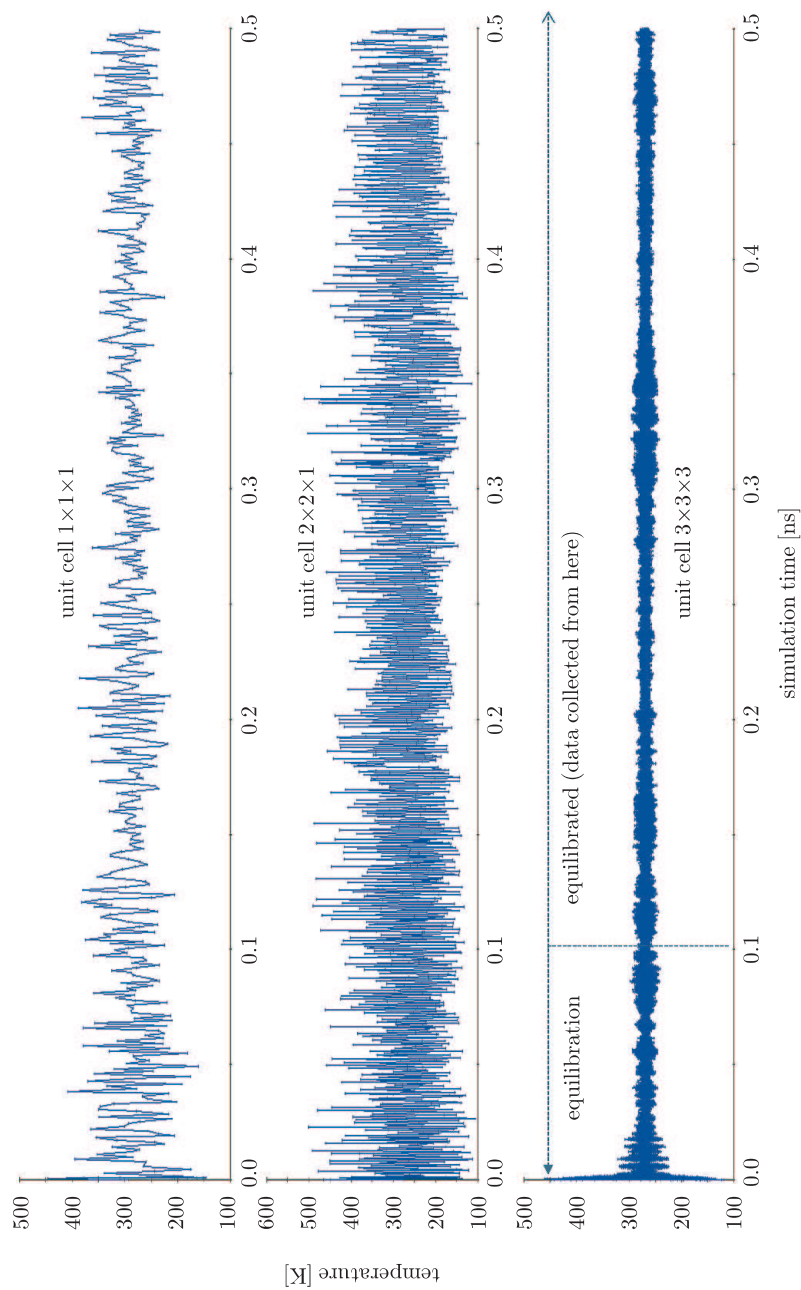


Figure 37. Plots of Temperature variation vs. simulation time

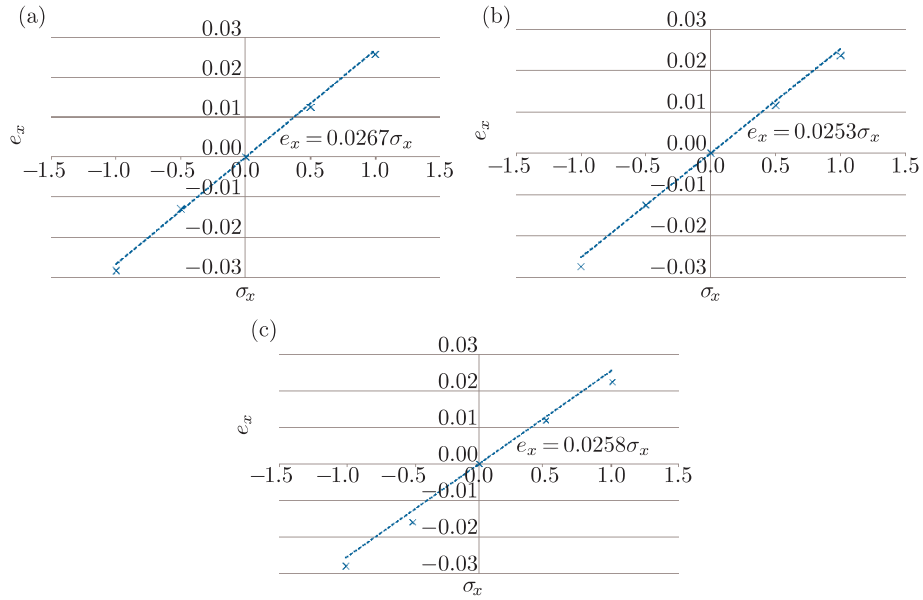


Figure 38. Plot of ϵ_x against s_x (blue; GPa) where $E_x = m^{-1}$; (a) $1 \times 1 \times 1$ system, (b) $2 \times 2 \times 1$ system, (c) $3 \times 3 \times 3$ system

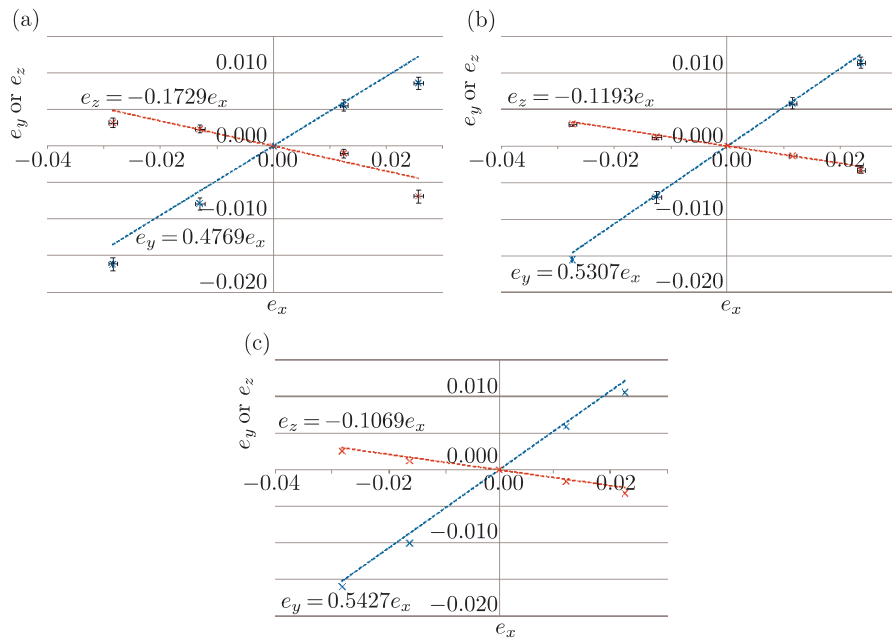


Figure 39. Plot of e_y vs. e_x (blue) and e_z vs. e_x (red) where n_{xy} and $n_{xz} = -m$ for the respective plots; (a) $1 \times 1 \times 1$ system, (b) $2 \times 2 \times 1$ system, (c) $3 \times 3 \times 3$ system



Table 6. Standard deviation of the lattice parameters at -1.0 , 0.0 and 1.0 GPa for all axis

	Lattice size	$\sigma_x = -1.0$ GPa	$\sigma_x = 0.0$ GPa	$\sigma_x = 1.0$ GPa
x	$1 \times 1 \times 1$	0.090	0.070	0.084
	$2 \times 2 \times 1$	0.082	0.146	0.086
	$3 \times 3 \times 3$	0.048	0.041	0.034
y	$1 \times 1 \times 1$	0.092	0.084	0.069
	$2 \times 2 \times 1$	0.105	0.138	0.115
	$3 \times 3 \times 3$	0.049	0.043	0.034
z	$1 \times 1 \times 1$	0.074	0.059	0.098
	$2 \times 2 \times 1$	0.022	0.023	0.034
	$3 \times 3 \times 3$	0.028	0.026	0.029

Table 7. The mechanical properties for loading in the x direction for all the systems simulated in this study

		v_{xy}	v_{xz}	E_x (GPa)
Dynamic	$1 \times 1 \times 1$	-0.48	0.17	37.45
	$2 \times 2 \times 1$	-0.53	0.12	39.53
	$3 \times 3 \times 3$	-0.54	0.12	38.76
Static		-0.57	0.12	36.63

were a larger deviation is observed in the $2 \times 2 \times 1$ unit cell, compared to the $1 \times 1 \times 1$ system. This may be due to the smaller possibility of movement for smaller unit cell sizes, than for the larger unit size, where the degree of freedom is larger. On the other hand it is evident that the $3 \times 3 \times 3$ has the lowest variation in its unit parameters, thus showing that the deviations observed in the lower unit sizes are probably due to erroneous calculations, brought about by their smaller unit sizes, and do not originate from adequate dynamic simulations. The limits of deviation of strain, observed in the graphs plotted for determination of Poisson ratios also provide further evidence that the deviation within the $3 \times 3 \times 3$ system is the least, although in the other systems only small deviations are observed.

The observation that results obtained by the larger unit cells are superior to the ones with small unit cells was to be expected since it is well known that larger unit cells give a better representation of what is occurring in real systems. This is due to the fact that in dynamic simulations, the atoms would be moving in a random manner subject to the potential energy restraints and the requirement imposed by the Maxwell-Boltzmann distribution for atomic velocities. However it should be noted that on increase of the lattice size used, there is a considerable increase in computational time. In fact, the $3 \times 3 \times 3$ system size took a lot of computational time, at least 7 days, thus this meant that proper analysis of larger systems, which should have been done in order to ensure that the $3 \times 3 \times 3$ size was adequate, were impractical to perform, due to time constraints. However, when

one considers the fact that the deviation within the parameters shown above was extremely small for this unit size, and also the fact that the Young's modulus and Poisson ratio for the unit cell size of $2 \times 2 \times 1$ and $3 \times 3 \times 3$ had a relatively close value, a larger unit size is expected to show that the systems size of $3 \times 3 \times 3$ was adequate. Computational time increase by a power rather than by a factor, for each increase in one direction, thus the time required for larger systems would have been too large and inadequate, and would most probably have shown the conclusions derived below.

If one compares the mechanical properties for loading in the x direction, one notes that values of the Young's modulus and Poisson ratios suggest that molecular dynamic simulations can reproduce the predicted auxeticity from the static studies (see Table 7).

An analyses of the mechanical properties data shows that there is very little discrepancy between the results obtained from dynamic simulations at different unit size, with the $3 \times 3 \times 3$ and $2 \times 2 \times 1$ results being practically identical. Also significant is the fact that despite the large variation in the instantaneous temperatures observed in the $1 \times 1 \times 1$ simulations the discrepancy between the mechanical properties obtained by these systems and those obtained for the larger systems was minimal. All this further suggests that there is no need to consider systems which are larger than $3 \times 3 \times 3$ as the system has adequately equilibrated and the mechanical property results have converged.

Also significant is the fact that the differences between the results obtained by the static simulations in the previous section and those obtained here are an excellent agreement, although the Young's moduli obtained from the dynamics simulations are slightly higher to that obtained from the static simulations whilst the Poisson's ratio n_{xy} is slightly less auxetic. Nevertheless, these discrepancies are not very high thus suggesting that for the system considered here, which consists of a well defined framework, the static simulation are adequate for simulating the mechanical properties including the predicted auxeticity. This is particularly true when one considers the much bigger variations that are observed when one uses different force-fields. The agreement between the two methods which are based on different methodologies also adds confidence to the results obtained and suggests that the methods are being implemented correctly.

Hence considering the slight differences between the mechanical properties of the systems, the fact that temperature variations of the larger system were much lower than the previous system, and that due to the exponential time increase for an increase in the system size, the $3 \times 3 \times 3$ system was chosen for further work, based on the results and discussion derived above, and on the assumption that a larger system would have increased the computational demand and result in relatively undetectable change, especially when one looks at the extremely small deviation within the strain for the $3 \times 3 \times 3$ system.

4.3. The deformation mechanism as simulated through MD

This section presents a more detailed analysis of the mechanism occurring within the system upon changes in stress. A full analysis aimed at obtaining the average dimensions related to the connected squares model as performed in the previous section so as to identify the deformation mechanism through dynamics simulations. The results obtained will be compared with the statics work.

4.3.1. Methodology

The $3 \times 3 \times 3$ system was established as the best choice for use in the following study by the study performed in the previous section. The frames extracted as .msi as described in the methodology, in addition to the cell projections, contained also the coordinates for all of the atoms within the system. Similar to the static simulation, a set of four squares is being considered for extraction of parameters elucidating the results, as seen in Figure 40.

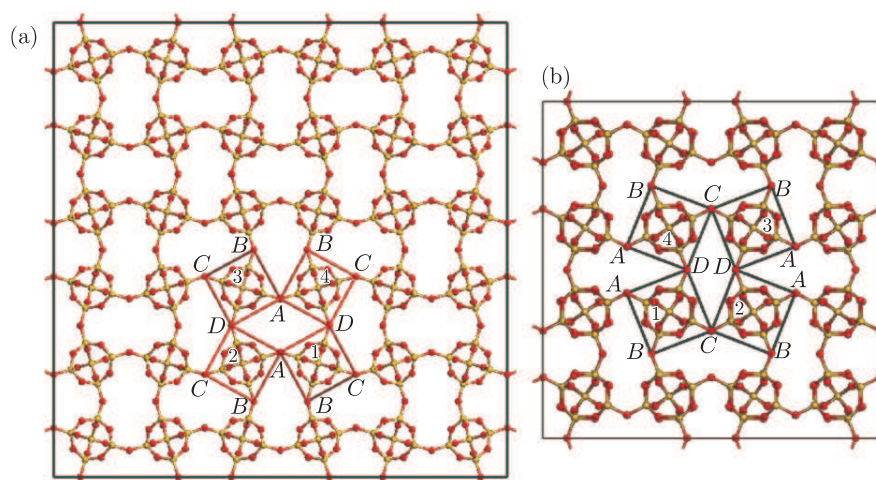


Figure 40. (a) The $3 \times 3 \times 3$ system and its coordinates; (b) the $2 \times 2 \times 1$ system used already in section 3 shown here for comparison

Being a dynamic simulation, each frame extracted from the run, represent an image of the system at that instant and to obtain true representation, these ‘instantaneous pictures’ should be viewed collectively. Thus, each frame extracted was incorporated in the final picture obtained. It should also be pointed out that given the size of the system; $3 \times 3 \times 3$, there are three repeat units along each axis, and thus along the z direction three of the considered units were present. The final picture also incorporated each of these three repeats within every time frame. This was done by averaging the coordinates in both time and spatial dimensions into one single point, thus resulting in a picture which considered both of these dimensions and changes occurring within.

4.3.2. Results and discussion

The results from this analysis are summarised in Tables 8–9. In particular, Table 8 shows a comparison of the structures at zero stress in terms of the ‘connected squares’ whilst Table 9 lists the changes occurring in the lattice as a whole and the parameters depicted in Figure 40 per GPa of applied stress, (obtained from gradients of the parameters *vs.* stress graphs, not shown). Shown also are a graph of the x , y and z projections as they vary over the simulation time (after the equilibration phase) so as to give an induction of variation in the properties measured (see Figure 37).

Table 8. A comparison of the structures at zero stress in terms of the ‘connected squares’

	Square (n)	Dynamic				Static			
		1	2	3	4	1	2	3	4
Sides	$A_n B_n$	4.93	4.93	4.93	4.93	4.93	4.93	4.93	4.93
	$B_n C_n$	4.93	4.93	4.93	4.93	4.93	4.93	4.93	4.93
	$C_n D_n$	4.93	4.93	4.93	4.93	4.93	4.93	4.93	4.93
	$A_n D_n$	4.93	4.93	4.93	4.93	4.93	4.93	4.93	4.93
Diagonals	$A_n C_n$	6.97	6.97	6.97	6.97	6.97	6.97	6.97	6.97
	$B_n D_n$	6.97	6.97	6.97	6.97	6.97	6.97	6.97	6.97
Angles	$D_n A_n B_n$	90.03	90.00	90.02	90.01	90.00	90.00	90.00	90.00
	$A_n B_n C_n$	90.00	89.99	90.00	90.01	90.00	90.00	90.00	90.00
	$B_n C_n D_n$	89.98	89.98	89.99	90.00	90.00	90.00	90.00	90.00
	$C_n D_n A_n$	89.99	90.03	89.99	89.98	90.00	90.00	90.00	90.00
Angle between diagonals	ϕ_n	90.04	90.00	90.03	90.00	90.04	90.04	90.04	90.04
Angles between squares	θ_n	58.90	58.88	58.87	58.86	56.63	56.63	56.63	56.63
	ψ_n	148.87	148.93	148.87	148.86	146.59	146.66	146.66	146.59

These results suggest that in general there is a good agreement between the shape of the structure in terms of the connected squares obtained from the statics and dynamics simulations. In particular the shapes and sizes of the individual squares are practically identical. The main difference lies in the angle between the squares which is simulated through the dynamic simulations as approximately 58° as opposed to 56° predicted by the static simulations. This increase in size may be expected given that the system is being simulated at 300 K, rather than in its static form which corresponds to 0 K. This opening up of the angle between the squares may explain the observation that the Young’s moduli obtained from the dynamics simulations are slightly higher to that obtained from the static simulations whilst the Poisson’s ratio n_{xy} is slightly less auxetic since the idealised ‘rotating squares’ model [45] suggests that in the idealised model, the Young’s modulus increases as the angle between the squares increases. Such an increase would also have an effect on the observed Poisson’s ration, In fact, as explained elsewhere by

Table 9. The changes occurring in the lattice as a whole and the parameters depicted in Figure 40 per GPa of applied stress, (obtained from gradients of the parameters *vs.* stress graphs, not shown) lattice parameters per GPa of stress in *x*

<i>n</i>	% fractional changes in length								Changes in the internal angles of the squares (°)								Changes in angles between two quadrilaterals (°)		
	$A_n B_n$	$B_n C_n$	$C_n D_n$	$D_n A_n$	$A_n C_n$	$B_n D_n$	$A_n B_n C_n$	$B_n C_n D_n$	$C_n D_n A_n$	$D_n A_n B_n$	$A_n B_n D_n$	$B_n C_n A_n$	$C_n D_n B_n$	$D_n A_n C_n$	$A_n B_n C_n$	$B_n C_n D_n$	$C_n D_n A_n$	$D_n A_n B_n$	θ_n
Dynamic	1	0.017	0.575	0.066	0.589	0.822	-0.199	0.603	-0.595	0.567	-0.575	-0.310	-0.310	-0.575	-0.310	-0.310	-0.310	7.357	7.084
	2	0.030	0.616	0.021	0.607	0.836	-0.199	0.588	-0.593	0.598	-0.593	-0.336	-0.336	-0.593	-0.336	-0.336	-0.336	6.175	6.425
	3	0.017	0.604	0.053	0.584	0.832	-0.203	0.598	-0.577	0.588	-0.609	-0.321	-0.321	-0.609	-0.321	-0.321	-0.321	7.339	7.081
	4	0.036	0.605	0.013	0.611	0.834	-0.202	0.589	-0.586	0.599	-0.602	-0.334	-0.334	-0.602	-0.334	-0.334	-0.334	6.190	6.440
Static	1	0.027	0.604	0.027	0.604	0.819	-0.189	0.578	-0.578	0.578	-0.578	-0.331	-0.331	-0.578	-0.331	-0.331	-0.331	7.433	7.187
	2	0.027	0.604	0.027	0.604	0.819	-0.189	0.578	-0.578	0.578	-0.578	-0.331	-0.331	-0.578	-0.331	-0.331	-0.331	6.278	6.526
	3	0.027	0.604	0.027	0.604	0.819	-0.189	0.577	-0.577	0.577	-0.577	-0.331	-0.331	-0.577	-0.331	-0.331	-0.331	7.433	7.187
	4	0.027	0.604	0.027	0.604	0.819	-0.189	0.577	-0.577	0.577	-0.577	-0.331	-0.331	-0.577	-0.331	-0.331	-0.331	6.278	6.526

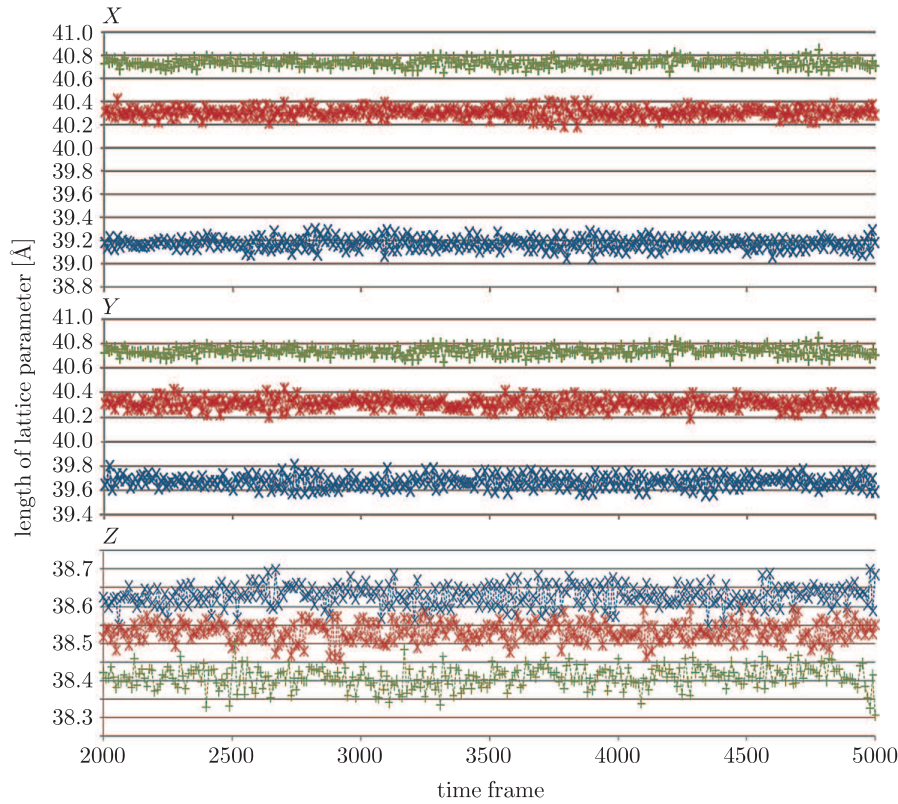


Figure 41. Plots of changes in length parameters along the x , y and z axis *vs.* time frame (note: these graphs show various interesting features, which were not that notable in static simulations, since instead of all of these values, only one value for the lattice parameters under a particular stress could be obtained; the first two graphs show the variation of the lattice parameters in the x and y direction under different stresses along the time frames;

it may easily be observed that the variation occurring is in fact as predicted; for a compression along the x axis there is a decrease in length along both axis, and an increase in length for a positive stress; this shows that the ν_{xy} is negative, while ν_{xz} is positive; this was as predicted by the static simulation, but what was not shown is that the actual change in length is sufficiently large for both axes, such that, there is no overlap between the lattice cell sizes at a difference in stress of 1 GPa, even over time and temperature variation)

Grima [13], when more than one deformation mechanism occur concurrently (as is the case in molecular level systems such as THO-SI), the an increase in the Young's modulus of one particular mechanism, will reduce its overall contribution to the total deformation. In other words, the opening up of the angles between the squares decreases the role of the 'rotating squares' mechanism which is responsible for the auxeticity with the net result the observed auxeticity decreases slightly.

The results show that the degree of change for any direction in the dynamic simulation is always lower than that for the static, this probably being a consequence of the decreased Young's modulus described above. There is also a lower change in the lattice dimensions in response to stress.

If one analysis the deformations of the squares and the angles between them, one notes that there is, to a first approximation, an excellent agreement between the two sets of result. This is very significant as the conclusions made in the previous section regarding the deformation mechanism were confirmed by this more elaborate simulation method. In particular, these simulations are confirming that by far, the largest degree of change is observed in the angle θ between the squares, hence showing that the most important deformation occurring within these systems, upon change in stress is once again from rotation of the squares over the Si-O-Si hinges. All this confirms the importance of this rotating mechanism. In addition to this, there are also small changes in the other parameters, emphasising the point that deformation in the squares do occur, and rotation of the squares is not the only change occurring within the system in response to stress, hence implying that other mechanisms do in fact interplay.

The ‘additional deformations’ observed here are of a similar nature to those described in the previous section, with minor discrepancies. For example, there is a larger increase in the diagonal AC compared to a smaller decrease in diagonal AB , immediately indicating that there is a more deformation of the squares as a result of the slightly reduced ability of the ‘rotating squares’ mechanism as a result of the increase in q from $c.56^\circ$ to $c.58^\circ$ described above, thus giving space for the additional deformation mechanisms. Also, the internal angles of the squares are observed to change slightly more in the dynamics as opposed to the statics simulations.

These considerations show that dynamic simulations have not proposed a different mechanism, but rather confirm the mechanism speculated by the static simulations. All of the comparisons between dynamic and static simulations though show some degree of difference. Overall the variations occurring in the parameters are fairly small, as can be observed, thus indicating, that although static simulations give the parameters as equivalent, which are not, as observed in the dynamic simulations, the degree by which they are different is in fact not large enough as to change the proposed mechanism, as noted previously.

On the other hand, this sets grounds for new studies, such as the deviations of atoms from an idealised minimum or average over time, during a simulation and also one may vary temperature in order to further show the degree of change of this variation over a difference in temperature.

Thus dynamic simulations give various advantages over static simulations, especially in elucidating what is happening within the structure upon application of stress and at different temperatures, allowing for a more realistic elucidation of a possible mechanism which may interplay during a change in a factor, such as stress or temperature.

4.4. Conclusion

From this section it may be concluded that the NPT dynamics simulations confirm that THO-SI is predicted to exhibit negative Poisson’s in the (001) plane which may be explained through a ‘rotating squares’ mechanism. In fact, the

results suggest the same mechanical properties, with a similar mechanism to the ones obtained through the much simpler and faster static simulations. Minor discrepancies between the two sets of simulations were also explained.

Given that the magnitude of the difference involved is relatively low, and given that when one compares the time required to generate these dynamic simulations it is obvious that the time required for the dynamic simulation, heavily outweighs the additional data and the more realistic simulation generated by this method, unless one needs to simulate properties which may not be obtained through static simulations, e.g. the temperature dependence of the mechanical properties.

4.5. Conclusions and further work

This paper has presented the results of new simulations performed on the siliceous equivalent of the THO framework aimed at predicting their mechanical behaviour. In particular, an attempt was made to reproduce the reported negative Poisson's ratio in the (001), as well as identifying the deformation mechanism which results in the particular values of the Poisson's ratios observed. These simulations were conducted through the COMPASS force-field, a force-field which had not been used before to simulate this framework. Furthermore, the simulations reported in this paper include a study conducted using Molecular Dynamics simulations, rather than simple minimisations, the technique used in all other studies on auxetic zeolites. Such technique has the advantage of simulating systems more realistically, taking in consideration factors, such as temperature variations.

The work presented here has shown that the COMPASS force-field is adequately parameterised to model THO-SI as it can predict the correct shape of framework and can predict mechanical properties which compare well to those found in the literature.

Both the statics and dynamics studies conducted using the COMPASS force-field can reproduce the predicted auxeticity for THO-SI, with the discrepancy between the two methods being smaller than the discrepancy that is obtained when one using different force-fields. This is very significant as it adds confidence to the results obtained using the two methodologies and confirms the suitability of minimisation-based techniques for simulating the mechanical properties. All this is very significant as we have now obtained significantly more evidence that THO-SI is indeed likely to be auxetic.

Also, both the statics and dynamics studies confirm that the COMPASS force-field is able to reproduce the prediction that the major mechanism that of rotating squares. It is also able to predict the less dominant mechanisms, such as that of deforming squares. Once again, this is very significant as for the first time there is evidence obtained through molecular dynamics for this deformation mechanism.

This work, apart from confirming the auxeticity of THO-SI and the mechanism responsible for it, is also very significant from the point of view that it

has developed a methodology for performing molecular dynamics on THO-type structures which can be used to obtain the mechanical properties and also, more importantly, the deformation mechanism. This is likely to open new avenues for the study of such systems which can only be performed through molecular dynamics. For example the study performed here has only considered the system at an ambient temperature of 300 K and ambient pressure. Previous studies have shown that the auxeticity in this type of frameworks is not at its maximum at ambient pressure conditions and in fact such systems can be made more auxetic if they are tested at non-ambient pressures [13]. It may be hypothesised that auxeticity may also be affected by temperature and thus it is important to simulate the mechanical properties of thomsonite and related systems at non-ambient conditions as was performed in the earlier pressure studies. However, whilst these pressure studies could easily be performed using static simulations, this is not the case for studying systems at various temperatures, which must necessarily be performed using molecular dynamics technique. In this respect, it would be desirable to perform simulations at different combinations of temperature and pressure so as to optimise the conditions required for maximum auxeticity.

In addition to this it is well known that structures involving rotating rigid units such as the ‘rotating squares’ model shown here can exhibit other interesting properties such as negative thermal expansion, a property which once again can only be studied using molecular dynamics, as it involves temperature as a parameter. Thus, it would be highly desirable if further work based on the methodology derived here could be carried out in an attempt to perform simulations aimed at seeing how the thermal expansion and Poisson’s ratio are related, with the hope of identifying materials which can exhibit both negative thermal expansion and negative Poisson’s ratio.

Further work may also be carried out using different force-fields, so as to ascertain that the results are not artefacts of the force-field used. Also comparison of force-fields may allow for establishment of the best force-field to be used in future studies. In order to obtain more robust results dynamic runs may be carried out more than once, averaging the results obtained between the runs, reducing the chances that any possible erroneous calculations affect the ultimate results.

References

- [1] Evans K E 1991 *Endeavour* **15** 170
- [2] Lakes R S 2001 *Phys. Rev. Letters* **86** 2897
- [3] Baughman R H, Stafstorm S, Cui C and Dantas S O 1998 *Science* **279** 1522
- [4] Barrera G D, Bruno J A O, Barron T H K and Allan N L 2005 *J. Phys.: Cond. Mat.* **17**, R217
- [5] Atfield M P and Sleight A W 1998 *Chem Commun.* **5** 601
- [6] Wojciechowski K W and Branka A C 1994 *Molecular Physics Reports* **6** 71
- [7] Alderson A 1999 *Chemistry and Industry* 384
- [8] McDonald S A, Ravirala N, Withers P J, Alderson A 2009 *Scripta Materialia* **60** 232
- [9] Evans K E, Alderson A and Christian F R 1995 *J. Chem Soc. Faraday Trans.* **91** 2671
- [10] Masters I G, Evans K E 1996 *Composite Structures* **35** 403

- [11] Attenborough F R 1997, Ph. D. Thesis, University of Liverpool
- [12] Grima J N, Zammit V, Gatt R, Alderson A and Evans K E 2007 *Auxetic behaviour from rotating semi-rigid units*, *Phys. Stat. Sol. (b)* **1**
- [13] Grima J N 2009 *Auxetic Materials*, In McGraw-Hill Yearbook of Science & Technology 41
- [14] Grima J N, Jackson R, Alderson A and Evans K E 2000 *Adv. Matter.* **12** 1912
- [15] Grima J N, Alderson A and Evans K E 2005 *Phys. Stat. Sol. (b)* **242** 561
- [16] Grima J N, Gatt R, Zammit V, Williams J J, Evans K E, Alderson A and Walton R 2007 *Journal of Applied Physics* **101** 86102
- [17] Gatt R, Zammit V, Caruana Ch and Grima J N 2008 *Phys. Stat. Sol. (b)* **245** (3) 502
- [18] Grima J N, Zammit V, Gatt R, Attard D, Caruana Ch and Chircop Bray T G 2008 *Journal of Non-Crystalline Solids* **354** 4214
- [19] Grima J N, Cassar R N and Gatt R 2009 *On the effect of hydrostatic pressure on the auxetic character of NAT-type silicates*, *J. Non-Cryst. Solids* **355** 1307
- [20] Lethbridge Z A D, Williams J J, Walton R I, Smith C W, Hooper R M and Evans K E 2006 *Acta Mater.* **54** 2533
- [21] Scarpa F, Panayiotou P and Tomlinson G 2000 *Journal of Strain analysis* **35** (5)
- [22] Yang W, Li Z-M, Shi W, Xie B-H and Yang M-B 2004 *J. Mater. Sci.* **39** 3269
- [23] Scarpa F, Adhikari S and Srikantha Phani A 2009 *Nanotechnology* **20** 65709
- [24] Grima J N, Alderson A and Evans K E 2005 *Physica Status Solidi B* **242** 561
- [25] Baughman R H and Galvao D S 1993 *Letters to Nature* **365** 735
- [26] Baughman R H, Galvao D S, Cui C and Dantas S O 1997 *Hinged and chiral polydiacetylene carbon crystals*, *Chemical Physics Letters* **269** 356
- [27] Lakes R S 1987 *Science* **235** 1038
- [28] Smith C W, Grima J N and Evans K E 2000 *Acta Materialia* **48** 4349
- [29] Grima J N, Gatt R, Sandre, Alderson A and Evans K E 2005 *IMECE* 82260
- [30] Gibson L J and Ashby M 1988 *Mechanics of cellular solids*, Pergamon
- [31] Nir Pour, Lior Itzhaki, Benaya Hoz, Eli Altus, Harold Basch, and Shmaryahu Hoz 2006 *Molecular Mechanics, Angew. Chem. Int. Ed.* **45** 5981
- [32] Nir Pour, Eli Altus, Harold Basch and Shmaryahu Hoz 2009 *J. Phys. Chem. C* **113** 3467
- [33] Grima J N, Gatt R, Chircop Bray T G, Alderson A and Evans K E 2005 *Molecular simulations* **31** (13) 925
- [34] Caddock B D and Evans K E 1989 *J. Phys. D: Appl. Phys.* **22** 1877
- [35] Alderson K L, Kettle A P, Neale P J, Pickles A P and Evans K E 1997 *Appl. Acoust.* **50** 23
- [36] Alderson K L, Fitzgerald A and Evans K E 2000 *J. Mater. Sci.* **35** 4039
- [37] Alderson K L, Alderson A and Evans K E 1997 *J. Strain. Anal. Eng.* **32** (3) 201
- [38] Grima J N, Williams J J and Evans K E 2005 *Chem Comm.* **32** 4065
- [39] Grima J N, Williams J J and Evans K E 2005 *Molecular Simulation* **31** 13
- [40] Chen L, Changhong L, Jiaping W, Wei Z, Chunhua H and Shoushan F 2009 *Auxetic materials with large negative Poisson's ratios based on highly oriented carbon nanotube structures*, American Institute of Physics
- [41] Wojciechowski K W 1989 *Physics Letters A* **137** 60
- [42] Lakes R S 1991 *J. Mat. Sci.* **26** 2287
- [43] Grima J N, Gatt R and Farrugia P-S 2008 *Phys. Stat. Sol. (b)* **1**
- [44] Sigmund O 1995 *Mechanics of Materials* **20** 351
- [45] Grima J N and Evans K E 2000 *Journal of Materials Science, Letters* **19** 1563
- [46] Grima J N, Zammit V, Gatt R and Evans K E 2006 *Phys Stat Sol. (b)* **224** 886
- [47] Evans K E and Alderson K L *Engineering Science and Education Journal, Materials* 148
- [48] He C, Liu P and Griffin A C 1998 *Macromolecules* **31** 3145
- [49] Poulter D R 1963, Oxford University Press Ch. 7
- [50] Bailey R W, Cox H A 1961 *GEC J.* **28** (72)

- [51] Muto K, Bailey R W and Mitchell K J 1963 *Proc. Inst. Mech. Eng.* **177** (155)
- [52] Rothenburg L, Berlin A A and Bathurst R J 1991 *Nature* **354** 470
- [53] Peter V Pikhitsa, Mansoo Choi, Hyung-Jung Kim and Sung-Hoon Ahn 2009 *Phys. Status Solidi B* **246** (9) 2098
- [54] Mancini G and Natali R. 2005 *Phys. Stat. Sol. (b)* **242** (3) 632
- [55] Rasburn J, Mullarkey P G, Evans K E, Alderson A, Ameer-Beg S and Perrie W 2001 *AIChE Journal* **47** (11) 2623
- [56] Baughman R H, Shacklette J M, Zakhidov A A and Strafstorm S 1998 *Nature* **392** 362
- [57] MSI Inc. 1997 *Cerius². User-guide-Force-field based simulations*
- [58] Rappe A K 1992 *J. Am. Chem. Soc.* **114** 10024
- [59] Mayo S L *et al.* 1990 *J. Phys. Chem.* **94** 8897
- [60] Burchart E *et al.* 1992 *Zeolites I* **12** 183
- [61] Gale J D 1997 *GULP* – „A computer program for the symmetry adapted simulation of solids”, *JCS Faraday Trans.* **93** 629
- [62] Hill J-R and Sauer J 1994 *J. Phys. Chem.* **98** 1238
- [63] Fleys M and Thompson R W 2005 *J. Chem. Theory Comput.* **1** (3) 453
- [64] Grima J N, Gatt R, Zammit V, Alderson A and Evans K E 2005 *Xjenja* **10** 24
- [65] Andersen H C 1980 *J. Chem. Phys.* **72** 2384
- [66] Berendsen H J C, Postma J P M, van Gunsteren W F, DiNola A and Haak J R 1984 *J. Chem. Phys.* **81** 3684
- [67] Nose S 1984 *Molec. Phys.* **52** 255
- [68] Nose S 1984 *J. Chem. Phys.* **81** 511
- [69] Nose S 1991 *Prog. Theoret. Phys. Supplement* **103** 1
- [70] Hoover W 1985 *Canonical Dynamics: equilibrium phase-space distributions*, *Phys. Rev.* **A31** 1695
- [71] Allen M P and Tildesley D J 1987 *Computer simulation of liquids*, Clarendon Press, Oxford Science Publications
- [72] Parrinello M and Rahman A 1981 *J. Appl. Phys.* **52** 7182
- [73] Coombs S D *et al.* 1997 *The Canadian Mineralogist* **35** 1571
- [74] Tschernich R W 1995 *Geoscience Press Phoenix*
- [75] Valyocsik *et al.* 1990 *US patent number 4,923,690 (May, 8, 1990)*
- [76] Xu R, Pang W, Yu J, Huo Q, and Chen J 2007 *Chemistry of Zeolites and Related Porous Material – Synthesis and Structure*, WILEY-VCH Verlag GmbH & Co. KGaA
- [77] Pluth J J, Smith J V and Kvik Å 1985 *Zeolites* **5** 74
- [78] Gatt R, Ph. D. University of Malta (in print)
- [79] Cerius², User Manuals (and references cited within), Accelrys Inc.
- [80] Ewald P P 1921 *Ann. Phys. (Leipzig)* **64** 253
- [81] IUPAC Quantities 1993 *Units and Symbols in Physical Chemistry. Second Edition*, Blackwell Scientific Publications
- [82] Zammit V 2007, University of Malta Msc. Thesis
- [83] Gatt R, Zammit V, Caruana Ch and Grima J N 2008 *Phys. Stat. Sol. (b)* **245** (3) 502
- [84] Kimizuka H and Kaburaki H 2000 *The American Physical Society, Physical Review Letters* **84** 24

